UNIVERSIDADE TECNOLÓGICA FEDERAL DO PARANÁ

ANDRESSA WILLE

WARPS INDUZIDOS PELA INTERAÇÃO COM SATÉLITES EM GALÁXIAS BARRADAS SIMULADAS

DISSERTAÇÃO

CURITIBA

2024

ANDRESSA WILLE

WARPS INDUZIDOS PELA INTERAÇÃO COM SATÉLITES EM GALÁXIAS BARRADAS SIMULADAS

Warps induced by the interaction with satellites in simulated barred galaxies

Dissertação apresentada como requisito para obtenção do título de Mestre em Física e Astronomia, do Programa de Pós-Graduação em Física e Astronomia, da Universidade Tecnológica Federal do Paraná (UTFPR).

Orientador: Prof. Dr. Rubens Eduardo Garcia Machado

CURITIBA

2024

ANDRESSA WILLE

WARPS INDUZIDOS PELA INTERAÇÃO COM SATÉLITES EM GALÁXIAS BARRADAS SIMULADAS

Trabalho de pesquisa de mestrado apresentado como requisito para obtenção do título de Mestre Em Física da Universidade Tecnológica Federal do Paraná (UTFPR). Área de concentração: Física .

Data de aprovação: 06 de Agosto de 2024

Dr. Rubens Eduardo Garcia Machado, Doutorado - Universidade Tecnológica Federal do Paraná

Dr. Alexandre Jose Tuoto Silveira Mello, Doutorado - Universidade Tecnológica Federal do Paraná

Dra. Karin Menendez Delmestre, Doutorado - Universidade Federal do Rio de Janeiro (Ufrj)

Dedico este trabalho a minha família.

AGRADECIMENTOS

É curioso pensar em como pequenas ações aleatórias e não planejadas podem mudar muitas coisas a longo prazo. Apesar de gostar de ciência e matemática desde criança, foi em fevereiro de 2015 que um insight inesperado me levou a escolher a astronomia como carreira. Eu tinha quase 15 anos e estava passeando com a minha família em uma cidade litorânea pequena, com um céu noturno bem mais limpo que o de Curitiba. A ação simples de observar o céu, algo que eu não dava muita importância antes, mudou alguma coisa em mim. Às vezes eu me pergunto se povos antigos, milhares de anos atrás, tiveram a mesma sensação ao olhar as estrelas. E, embora eu busque tomar decisões racionais na maior parte do tempo, alguns sentimentos são muito difíceis de ignorar, então eu passei os últimos nove anos estudando astronomia, primeiro como hobby e agora como profissão. Isso obviamente teve impacto na minha carreira acadêmica, mas também influenciou minha vida pessoal, pois me fez conhecer pessoas importantes, que eu gostaria de agradecer aqui. São muitas, então o texto vai ser longo.

Em primeiro lugar, gostaria de agradecer ao meu orientador, Prof. Dr. Rubens Machado, por ser minha fonte de inspiração diária e meu principal guia nos últimos anos. Quando eu assisti uma palestra sua no começo de 2019, eu tive certeza absoluta de que você seria meu orientador. Agora, cinco anos depois, tendo trabalhado com você na iniciação científica e no mestrado, fico feliz em saber que minha intuição estava certa. Eu sou muito grata pela paciência, ternura e cuidado que você sempre teve comigo. Obrigada por me ensinar tanto, por sempre estar presente para tirar minhas dúvidas e corrigir meus trabalhos, e por me apoiar em processos burocráticos como a inscrição da iniciação científica no LIneA e o aceite da bolsa de mestrado. Você me deu liberdade e apoio para que eu pudesse aprender, errar e expressar minhas opiniões sem medo de ser julgada. Esse tipo de permissão é o presente mais valioso que alguém pode me dar.

Eu também quero agradecer minha família: minha mãe, meu pai e minha irmã, por terem abraçado minhas ambições. E nós sabemos que foram muitas. Eu tive muita sorte de crescer em meio a tantos privilégios e oportunidades de explorar todo tipo de conhecimento: nunca me faltaram livros de ciência, romance e fantasia; ou material para arte, culinária, jardinagem e costura; ou acesso a cursos de idiomas, dança, canto, fotografia, entre várias outras coisas que eu fui inventando ao longo dos anos. Explorar tudo isso me fez ser curiosa e escolher a ciência como carreira, mas sempre admirando outras áreas do conhecimento humano. Por tudo isso e por todas as caronas, refeições, proteção e apoio incondicional, obrigada papai, mamãe e Amanda.

Amo vocês.

Agradeço aos amigos que fiz durante a iniciação científica e mestrado na UTFPR: Elvis, Richards, Giovanni, Vinicius, Gustavo, Nicholas, Micheli, Caroline e Alexandre. E da iniciação científica no LIneA, Gabriel. Obrigada por todas as conversas, piadas e companhia para viagens. Agradeço também aos meus amigos da graduação, Aretha, Dani, André e Henrique. Apesar de estarmos todos seguindo carreiras diferentes, espero poder manter nosso vínculo por muitos e muitos anos. Por último, obrigada as minhas amigas de sempre (algumas há mais de 10 anos): Nath, Carol, Bruna, Lívia, Isabely, Maria e Duda. Tenho muita sorte em ter conhecido vocês e mais sorte ainda por vocês aguentarem minhas bobagens há tanto tempo.

Obrigada também a todos os professores e instituições que fizeram parte da minha jornada acadêmica até aqui. Eu sou especialmente grata ao Prof. Dr. João Steiner (*in memoriam*), pois as aulas de astronomia disponibilizadas no YouTube foram meu primeiro contato com a área de forma mais acadêmica, depois que eu já tinha explorado muito conteúdo de divulgação científica. Eu assisti essas aulas enquanto estava no ensino médio e isso me marcou muito. Destaco também um agradecimento especial ao meu professor de geografia do ensino médio, Laércio, que inscreveu o meu colégio na Olimpíada Brasileira de Astronomia e Astronáutica só porque eu pedi e ainda me emprestou material para que eu pudesse estudar para a prova. Esse incentivo foi mais importante para mim do que a medalha que eu ganhei naquele ano. Também sou grata aos professores que ministraram as disciplinas do mestrado e contribuíram muito para a minha formação: professores Rubens, Felipe, Alexandre, Marcelo Emílio e Jean. Em um mundo cheio de pseudociências e teorias da conspiração, é um alívio estar cercada por pessoas críticas e racionais. Agradeço também à banca pela disponibilidade de ler meu trabalho.

Ao Laboratório Interinstitucional de e-Astronomia (LIneA), muito obrigada por terem me escolhido como estudante de iniciação científica, dentre dezenas de outros jovens brasileiros. Ainda na graduação, eu aprendi muito sobre programação, inglês e astronomia no projeto desenvolvido e tive a maravilhosa oportunidade de participar do meu primeiro congresso internacional. Tudo isso me ajudou bastante no mestrado. Obrigada Julia e Michel por me orientarem tão bem.

Este trabalho foi realizado com o apoio da Coordenação de Aperfeiçoamento de Pessoal de Nível Superior (CAPES) - Código de Financiamento 001, e do Conselho Nacional de Desenvolvimento Científico e Tecnológico (CNPq). Agradeço pela bolsa e pelo suporte técnico.

E por último, agradeço ao povo brasileiro, que paga impostos todos os dias em

mercadorias, bens e serviços. Uma parte do arrecadamento desses impostos financia a educação pública brasileira e mantém toda a estrutura necessária para a minha carreira. Eu espero dar um retorno satisfatório ao investimento de vocês.

L'Astronomie est utile, parce qu'elle nous élève au-dessus de nous-mêmes; elle est utile, parce qu'elle est grande; elle est utile, parce qu'elle est belle.

(Poincaré, 1911)

RESUMO

WILLE, Andressa. **Warps induzidos pela interação com satélites em galáxias barradas simuladas**. 2024. 74 f. Dissertação (Mestrado em Física e Astronomia) – Universidade Tecnológica Federal do Paraná. Curitiba, 2024.

Warps são assimetrias verticais comuns que aparecem nas partes mais externas dos discos galácticos, curvando uma parte para cima e a outra para baixo. Muitos mecanismos podem desencadear a formação de warps, incluindo forças de maré. As interações com os satélites distorcem principalmente as bordas do disco e podem também alterar a morfologia central, tendo impacto, por exemplo, no desenvolvimento de uma barra galáctica. Em eventos de fusão, a barra pode ser enfraquecida ou mesmo destruída. Neste estudo, o objetivo é comparar modelos de galáxias barradas e não-barradas e a sua suscetibilidade à formação de warps. Para analisar os efeitos de warps induzidos, foram utilizadas simulações de N-corpos de uma galáxia central barrada e outra não barrada interagindo com satélites de várias massas ($0.1 \times 10^{10}\mathrm{M}_{\odot}$, $0.5 \times 10^{10}\mathrm{M}_{\odot}$ e $1 \times 10^{10}\mathrm{M}_{\odot}$) e raios orbitais iniciais (10, 20 e 30 kpc). Também foram realizadas simulações isoladas das galáxias centrais para comparação. Um dos resultados obtidos foi que as deformações induzidas são mais fortes na galáxia barrada em comparação com a galáxia não barrada, em modelos perturbados e isolados. Além disso, as massas dos satélites determinam o nível de destruição da barra e a intensidade do warp induzido. O momento em que a barra será enfraquecida ou destruída depende do raio orbital do satélite.

Palavras-chave: galáxias barradas. warps. satélites. simulações de N-corpos.

ABSTRACT

WILLE, Andressa. **Warps induced by the interaction with satellites in simulated barred galaxies**. 2024. 74 p. Dissertation (Master's Degree in Physics and Astronomy) – Universidade Tecnológica Federal do Paraná. Curitiba, 2024.

Warps are common vertical asymmetries that appear in the outer parts of the galactic discs, bending one part upwards and the other downwards. Many mechanisms can trigger warp formation, including tidal interactions. The interactions with satellites distort mainly the edges of the disc and can also change the central morphology, impacting, for example, the development of a galactic bar. In mergers events, the bar can be weakened or even destroyed. In this study, we aim to compare barred and non-barred galaxy models and their susceptibility to warping. To analyze the effects of induced warps, we used N-body simulations of a barred and a non-barred central galaxy interacting with satellites of varying masses ($0.1 \times 10^{10} M_{\odot}$, $0.5 \times 10^{10} M_{\odot}$ and $1 \times 10^{10} M_{\odot}$) and initial orbital radii (10, 20 and 30 kpc). We also ran isolated simulations of the central galaxies for comparison. We found that the induced warps are stronger in the barred galaxy compared with the non-barred galaxy, in perturbed and isolated models. In addition, the masses of the satellites determine the level of destruction of the bar and the intensity of the induced warp. The time in which the bar will be weakened or destroyed depends on the orbital radius of the satellite.

Keywords: barred galaxies. warps. satellites. N-body simulations.

LISTA DE FIGURAS

LISTA DE TABELAS

LISTA DE ABREVIATURAS, SIGLAS E ACRÔNIMOS

SIGLAS

AGN	Active Galaxy Nuclei
EHT	Event Horizon Telescope
ESA	European Space Agency
JWST	James Webb Space Telescope
LSST	Legacy Survey of Space and Time
SMBH	Supermassive Black Hole
SPH	Smoothed-Particle Hydrodynamics

ACRÔNIMOS

GADGET	GAlaxies with Dark matter and Gas intEracT

SUMÁRIO

1 INTRODUCTION

Galaxies are associations of stars, gas and interstellar dust, surrounded by dark matter. Galactic astronomy is the study of our own galaxy, the Milky Way, and extragalactic astronomy is the study of other galaxies and their characteristics, structures and interactions. This chapter will first explain a brief history of extragalactic astronomy, then will discuss the properties of spiral galaxies, as well as current challenges in this area. The last sections focus on specific morphological aspects of galaxies: bars and warps.

1.1 EXTRAGALACTIC ASTRONOMY

Despite the ancient thinkers already reflecting on the organization of the universe into large collections of stars, extragalactic astronomy has been developed since the 20th century. Until then, other galaxies (at the time, called "nebulae") were considered to be part of the Milky Way. With the equipment and methods used at the time, it was difficult to distinguish the morphological structures of galaxies because of their diffuse appearance and determining distances was also a challenge. Over the years, better telescopes have been developed and determining distances has become easier with the relation between the pulsation period and the absolute magnitude of Cepheids, measured by Henrietta Leavitt (1908).

In the 1920s, the "Great Debate" divided the opinion of astronomers about the scale of the Universe (SHAPLEY; CURTIS, 1921): Harlow Shapley believed that the Milky Way was very large ("Big Galaxy") and all the "spiral nebulae" were inside it, but Heber Curtis argued that the Milky Way and these "nebulae" were separate objects. A few years later, Edwin Hubble calculated the distance of M31 (Andromeda galaxy) using Cepheids (HUBBLE, 1929). The conclusion was that the "spiral nebulae" were very far from the Milky Way, and they were actually other galaxies (SMITH, 2008; SMITH, 2009).

In the following decades, other aspects of galaxies have begun to be studied. The high velocity dispersions in galaxy clusters and flat rotation curves in spiral galaxies indicated masses larger than expected, and this unobservable matter became known as dark matter (SWART; BERTONE; DONGEN, 2017). Although these discoveries were made between the 1930s and 1970s, the nature of the dark matter remains unknown.

The study of galaxy spectra had been improved, and with the advance of radio astronomy in the 1950s, very energetic sources (Seyfert galaxies, radio galaxies, quasars and others) were discovered (SHIELDS, 1999). The discovery that these were all manifestations of the same phenomenon took many years. The unified model established that these objects are active galaxy nuclei (AGN), and the energy source is a supermassive black hole (SMBH).

All these advances in extragalactic astronomy have led to new questions that are still open. A current challenge in this area is a more complete understanding of the evolution of galaxies, considering their structures, interactions and formation (CONSELICE, 2014; MARZIANI, 2015). Investigating our own galaxy is also a challenge because of our position within the galactic disk. Various other aspects, such as the nature of dark matter or the behavior of black holes in the center of galaxies are not completely understood either, and involve knowledge from astronomy and several areas of physics.

Over the last few years, there has been a significant investment in new instruments. Gaia (GAIA COLLABORATION *et al.*, 2016) is an astrometry telescope from the European Space Agency (ESA) that has been mapping more than a million stars in the Milky Way over the last decade. The James Webb Space Telescope (JWST), launched in 2021, is bringing innovations in high-redshift galaxy observations (ROBERTSON, 2022), for example. And the upcoming Legacy Survey of Space and Time (LSST) data from the Vera Rubin Observatory (in construction) will also bring new data on different areas. Particularly in galactic and extragalactic astronomy, some of the goals are mapping the Milky Way and probing dark matter (IVEZIĆ *et al.*, 2019). In addition, new algorithms for analyzing data are constantly emerging.

1.2 SPIRAL GALAXIES

Since the discovery of other galaxies beyond the Milky Way, our knowledge about these objects has developed rapidly. Galaxies can be found in groups (containing a few dozen galaxies) and clusters (containing hundreds to thousands of galaxies) and they can have different shapes, sizes and masses. The wide variety of morphologies has been studied since the beginning of the development of extragalactic astronomy. These aspects are still relevant in current investigations, because studying the structure and features of galaxies leads to a better understanding of the dynamic processes they have undergone (CONSELICE, 2014).

Hubble (1936) created a classification system containing basic morphologies of galaxies: elliptical, lenticular, spiral and irregular, as illustrated in Figure 1. In terms of shape, elliptical galaxies (“E”) are spheroidal; spiral galaxies (“S”) are disk-shaped with spiral patterns and can have a bar ("SB"); lenticular galaxies ("S0") also have a disk shape but without spiral arms, and irregular galaxies ("Irr") have peculiar shapes that don't fit into the other classifications. The classification system was modified and extended by Vaucouleurs (1963), who added more categories, such as "Sd" spirals and weakly barred spirals "SAB". These additional categories are not shown in the figure.

Using this type of diagram, galaxies are generally divided into early-type (ellipticals and lenticulars) and late-type (spirals and irregulars). It is also common to classify spiral galaxies into early-type (Sa and Sb) and late-type (Sc and Sd) spirals. But it is important to note that these denominations and the Hubble diagram do not determine a evolutionary sequence of galaxies. The Hubble diagram is useful for illustrating the variety of galaxies in the Universe: for example, elliptical galaxies can have a lower ("E0") or higher ("E7") degree of ellipticity, and spiral galaxies can have their arms closer to the center ("Sa" and "SBa") or not ("Sc" and "SBc"). Over the years, the classification became more complete, considering rings, lenses and other internal structures. However, this classification by visual inspection depends on the orientation of the galaxies, and certain angles can make it difficult to identify and describe features. In the figure, the spiral galaxies are seen face-on, showing the spiral arms and the bar clearly, for example.

Figure 1 – Hubble's galaxy classification.

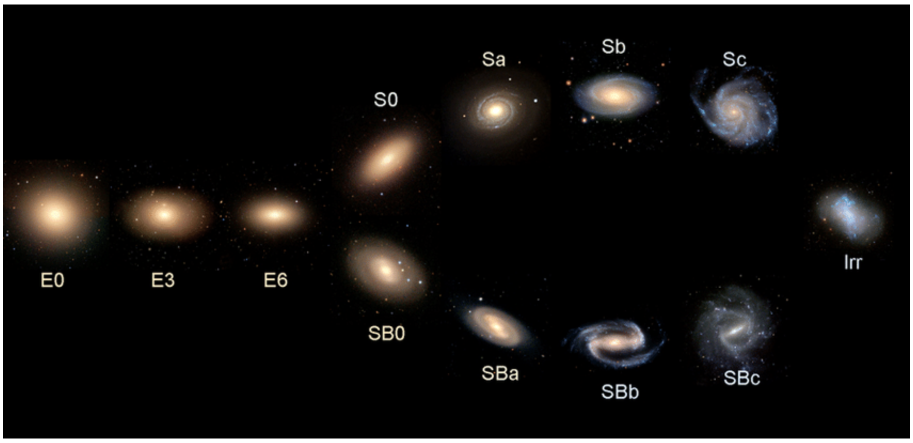

Source: Cui *et al.* (2014).

Spiral galaxies represent the majority of massive galaxies at low redshift (e.g NAIR; ABRAHAM, 2010a). The main feature that differentiates them from other types of galaxies is the presence of spiral arms, known as active sites of star formation in response to shock waves in these regions (ROBERTS, 1969). The majority of these galaxies have two spiral arms, but the number and the symmetry between them vary from galaxy to galaxy (HART *et al.*, 2016). The Milky Way is a spiral galaxy with four arms (e.g. HOU; HAN, 2014). One of the most popular theories about the mechanisms of spiral arm generation is the density wave theory (LIN; SHU, 1964), which proposes that spiral patterns in galaxies are caused by stationary density waves. Spiral arms are not rigid mass concentrations, but the galactic disk has areas of higher density that rotate with a particular pattern speed. Stars and gas move through these regions, where there is compression by shock waves, and then move out of them. In this model, density waves are self-driven, but there is also the theory that spirals can be caused by tidal interactions (e.g. TOOMRE; TOOMRE, 1972).

Spiral galaxies are formed by a disk of stars and gas, a close-to-spherical bulge in the center, and a dark matter halo which surrounds the galaxy. The scheme of Figure 2 shows these components in the Milky Way, viewed edge-on. The disk, where the spiral arms are formed, is composed by stars, gas and dust. In the figure, the position of the Sun is indicated at $R_{\odot} \approx 8.3$ kpc (BRUNTHALER *et al.*, 2011) from the galactic center. It also shows the division into thin disk and thick disk: they differ in terms of the scale height and stellar population. In edge-on late-type galaxies, the scale height of thick disks is ~ 2 times larger than thin disks (YOACHIM; DALCANTON, 2006). In addition, thick disk stars are generally older, have lower metallicity and higher dispersion velocities than thin disk stars (GILMORE; REID, 1983). The evolutionary history, stellar chemistry and kinematics of these parts of the disk still have many unresolved questions.

In the center of spiral galaxies, there is a close-to-spheroidal region called the bulge. Classical bulges look similar to elliptical galaxies in shape, kinematics and surface brightness profile. In Figure 2, the central region also involves the nucleus of the Milky Way, which is the supermassive black hole Sagittarius A^*. The first image of it was made by the Event Horizon Telescope (EHT) recently (EVENT HORIZON TELESCOPE COLLABORATION *et al.*, 2022).

Finally, the galactic halo is formed mainly by dark matter, but also contains clouds of neutral hydrogen and older stars concentrated in globular clusters. The dark matter only interacts with baryonic matter gravitationally and, as there is no electromagnetic interaction, we are unable to see it and determine its properties. Despite this, it is known that dark matter is an important component of galaxies, in fact, it contains most of their mass, as demonstrated by the flat rotation curves of spiral galaxies first measured by Rubin and Ford (1970), Rogstad and Shostak (1972). Rotation curves are useful tools in astronomy and can be used to estimate galaxy masses. As they relate the orbital velocity of the stars to the galactic radius, it is expected that the curve will decline at larger radii, but the measurements showed that this does not occur. This implies more mass than we observe. The dark matter is an invisible mass currently understood to be essential for the formation and evolution of galaxies.

At the bottom of the Hubble diagram (Figure 1), another important structure appears in some spiral galaxies: the bar. Barred spiral galaxies are denoted by “SB”. Although not shown in Figure 2, the Milky Way also has a bar in its center. Bars will be discussed further in the next section.

Figure 2 – Structure of the Milky Way.

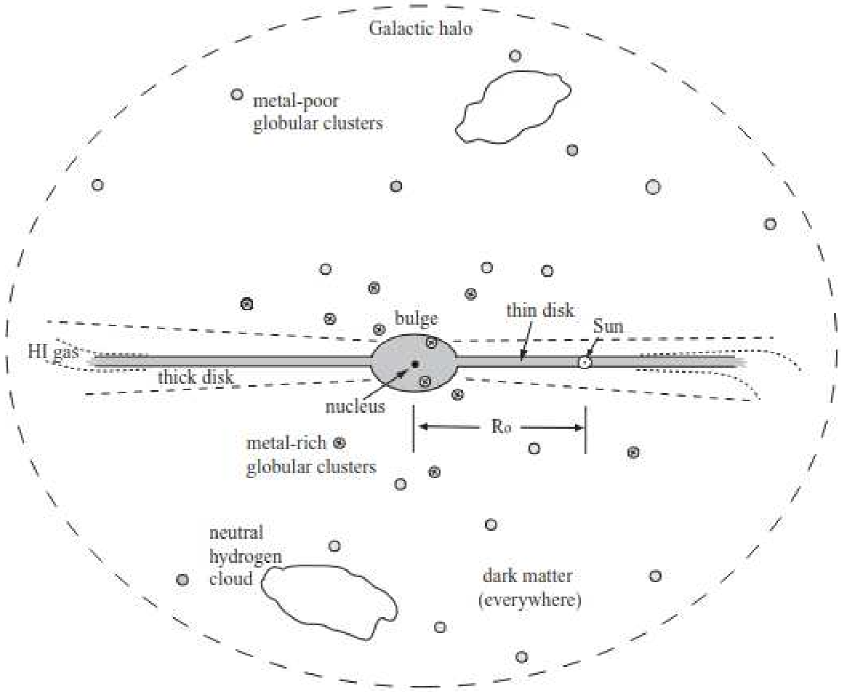

Source: Sparke and Gallagher (2007).

1.3 BARRED GALAXIES

Bars are elongated stellar structures in the center of the galactic disk, and they can have different masses, shapes, and kinematics. Nearly 60 per cent of spiral galaxies are barred (ESKRIDGE *et al.*, 2000; MENÉNDEZ-DELMESTRE *et al.*, 2007; SHETH *et al.*, 2008; LEE; ANN; PARK, 2019) when observed in near infrared. At optical wavelengths, the fraction is slightly smaller, around 50 per cent (MARINOVA; JOGEE, 2007; BARAZZA; JOGEE; MARINOVA, 2008). Studies show that bar fraction, i.e. the number of barred galaxies in a sample of galaxies, depends on the Hubble type (e.g. AGUERRI; MÉNDEZ-ABREU; CORSINI, 2009), the galaxy mass (e.g. NAIR; ABRAHAM, 2010b; SODI, 2017; ERWIN, 2018), and the environment (e.g. MÉNDEZ-ABREU *et al.*, 2012). The fraction of barred spirals also declines in higher redshifts

(SHETH *et al.*, 2008), although more recent JWST studies point to significant amount of bars at $z > 1-4$ (GUO *et al.*, 2023; COSTANTIN *et al.*, 2023; CONTE *et al.*, 2024). Figure 3 shows an example of barred galaxy: NGC 1300 is a spiral barred galaxy that belongs to the Eridanus cluster.

Figure 3 – Barred Spiral Galaxy NGC 1300.

Source: https://hubblesite.org

Aspects about the formation and evolution of this structure have been investigated for a long time. The Toomre Q parameter (TOOMRE, 1964) reveals the tendency of a galactic disk to have instabilities. A dynamically hot disk remains stable, axisymmetric, while a dynamically cold disk is unstable and tends to develop a bar. In addition, early studies using analytical methods and N-body simulations of isolated galaxies (e.g. HOHL, 1971; OSTRIKER; PEEBLES, 1973; WEINBERG, 1985) showed that bars form via the exchange of angular momentum between the inner disk and the halo or outer disk: circular orbits in the center of the galaxy become more elongated, losing angular momentum and forming the bar. The study of resonances and star orbits in the central region of galaxies has also helped to understand the kinematics of bars (e.g. ATHANASSOULA *et al.*, 1983; PFENNIGER, 1984).

As the N-body simulations evolved, it became clear that the evolution of bars strongly depend on the physical properties of the galaxy and its components. The spheroidal components, the halo and the bulge, seem to have a major influence. The bar strength can be impacted by the amount of angular momentum exchanged with them (ATHANASSOULA, 2003b) and by the halo central concentration (ATHANASSOULA; MISIRIOTIS, 2002), for example. Strong bars are also preferentially formed in galaxies with spherical (ATHANASSOULA; MACHADO; RODIONOV, 2013), live halos (represented by particles, in contrast to rigid halos that are represented by analytical potentials) (ATHANASSOULA, 2002; SELLWOOD, 2016). Besides the strength of the bar, other parameters, such as the rotation rate, can be affected by the dynamical friction from a dense halo (DEBATTISTA; SELLWOOD, 1998; DEBATTISTA; SELLWOOD, 2000).

The gas in the galactic disk is another factor that has an impact on the properties of the bar. In gas-rich disks, the bar is weaker and grows at a slower rate than in gas-poor disks (ATHANASSOULA; MACHADO; RODIONOV, 2013). Bournaud, Combes and Semelin (2005) argued that the gravitational torques exerted by gas on the bar weaken it. These torques misalign the stellar orbits, making them rounder and weakening the bar. Villa-Vargas, Shlosman and Heller (2010) found that, in addition to limiting the growth of the bar, the presence of the gas affects its pattern speed evolution (the rotational frequency of the bar).

On the other hand, the formation of the bar redistributes mass and angular momentum, impacting on the evolution of other components of the galaxy. It can lead to a loss of halo triaxiality (MACHADO; ATHANASSOULA, 2010), impact in the gas distributions in central parts of the galaxies (SAKAMOTO *et al.*, 1999; SHETH *et al.*, 2005) and transport material towards the center of AGN galaxies (e.g. ALONSO; COLDWELL; LAMBAS, 2014; SILVA-LIMA *et al.*, 2022), affecting its activity. The secular evolution of the disk is also influenced by the bar evolution (e.g. VALENZUELA; KLYPIN, 2003; DEBATTISTA *et al.*, 2006). During their secular growth, strong bars go through a short moment of instability associated with a sudden weakening and thickening. This particular phenomenon is known as bar buckling (COMBES; SANDERS, 1981; RAHA *et al.*, 1991; MARTINEZ-VALPUESTA; SHLOSMAN, 2004), probably driven by the vertical resonances of the stellar orbits in the bar (ŁOKAS, 2019a), and it can occur more than once (MARTINEZ-VALPUESTA; SHLOSMAN; HELLER, 2006). This event leads to the formation of a boxy/peanut structure in the galaxy center.

Methods of detecting bars and measuring their properties, such as shape and length, include elliptical isophote fitting (WOZNIAK *et al.*, 1995; ERWIN, 2005; MARINOVA; JOGEE, 2007); Fourier analysis of luminosity profile (ELMEGREEN; ELMEGREEN, 1985; AGUERRI *et al.*, 2000); and photometric decomposition of the surface brightness distribution (PRIETO *et al.*, 2001). The bar strength can also be measured by different methods, and one of the most common is the use of the $m = 2$ Fourier mode of the projected mass distribution (ATHANASSOULA; MISIRIOTIS, 2002; ATHANASSOULA; MACHADO; RODIONOV, 2013; PESCHKEN; ŁOKAS, 2018; ŁOKAS, 2019b; CUOMO *et al.*, 2019). However, the study of the bars has limitations and difficulties: the variation in bar fractions at different wavelengths and the orientation of the galaxy can make it difficult to identify these structures. The Milky Way also has a bar that is difficult to observe due to our position in the galaxy and the dust extinction (SHEN; ZHENG, 2020). Despite this, it is known that the Milky Way has a peanut-shaped bar with half-length of $\sim$ 5 kpc (WEGG; GERHARD; PORTAIL, 2015), viewed nearly end-on, with a bar angle of $\sim$ 25°- 30° (SHEN; ZHENG, 2020).

In simplified models, it is common to study the internal parameters that lead to the evolution of the bar in isolated galaxies, but the influence of the interactions of companion and satellites galaxies must also be examined. Méndez-Abreu *et al.* (2012) compared the bar fraction and properties at three different environments: the field, the Virgo cluster and the Coma cluster. They found differences in bar fractions at these environments and concluded that interactions can trigger or inhibit the bar formation, depending on the luminosity (and consequently, the mass) of the galaxies. While the brighter galaxies maintain their structure despite the close interactions, fainter galaxies are more fragile. They also suggest that bar formation mainly occur in pre-cluster stages, in galaxies in small groups. Other studies indicate that tidal induced bars are formed depending on the orbital configuration. Prograde encounters (in which the angular momenta of the disks are aligned) in equal-mass flybys induce strong bars, because tidal force acts for a longer time on the stars in the prograde galaxy than on the retrograde one (ŁOKAS, 2018). In addition, bars are induced more easily when the interaction occurs with a small pericentre distance or if the perturber is more massive (PESCHKEN; ŁOKAS, 2018).

Bars can also be destroyed. Bar dissolution can occur because of the internal characteristics of the galaxy: for example, if the galaxy has central mass concentrations, such as supermassive black holes, large condensations of molecular gas and star clusters (e.g. DAS *et al.*, 2003; SHEN; SELLWOOD, 2004; HOZUMI, 2012), or if the galaxy is in a prolate halo (IDETA; HOZUMI, 2000). The role of the environment is also important. Interactions with satellites can cause bar weakening in the case of minor merger events, because of the accumulation of stars (previously belonging to the satellite) in the central region of galaxy (GHOSH *et al.*, 2021). And if massive satellites collide with the disk, the bar is destroyed (ATHANASSOULA, 2003a). In dense environments, and depending on the intensity of the interaction, not only the bar is dissolved, but the disk is also destructed, resulting in morphological transformation of the galaxies (ROSAS-GUEVARA *et al.*, 2024). However, Zana *et al.* (2018) argues that bars can be resilient: unequal-mass encounters can weaken the bar, but it is recovered after the interaction.

1.4 WARPS

Bars are not the only asymmetries that spiral galaxies can exhibit. It is common for spiral galaxies to have distortions, such as polar rings (rings rotating almost perpendicularly to the disk of the galaxy), and lopsidedness (a side of the disk is more elongated than the other). Another important morphological asymmetry are warps. They are asymmetries in the galactic disk, where the amplitude increases with radius. The most common kind is the S-shaped or “integral sign” warp, as shown in Figure 4, but U-shaped warps or more complex structures can also appear (GÓMEZ *et al.*, 2017). In S-shaped warps, one side of the disk is tilted upwards and the other downwards, whereas in U-shaped warps, the disk curves into a bow shape. The degree of warping can vary and the warped disks can have asymmetries in amplitude and shape between the two sides. This difference are more pronounced in rich environments (GARCÍA-RUIZ; SANCISI; KUIJKEN, 2002).

Figure 4 – Warped galaxy ESO 510-G13.

Source: https://hubblesite.org

Detecting warps is not a trivial task, since they can only be seen when observing edge-on galaxies, and even with this orientation, not all angles are ideal for detection and measurements. In addition, tilted structures can be contaminated by dust or projected spiral arms (RESHETNIKOV; COMBES, 1998). Despite this, surveys of HI (neutral atomic hydrogen) 21 cm detected warp signals in several galaxies in the 1970s (BINNEY, 1992), and since then, many observational studies have been carried out, in the optical and in the HI. They have shown how common this type of structure is, representing more than half of the nearby edge-on galaxies (SÁNCHEZ-SAAVEDRA; BATTANER; FLORIDO, 1990; RESHETNIKOV; COMBES, 1998;

GARCÍA-RUIZ; SANCISI; KUIJKEN, 2002; ANN; PARK, 2006). Observations at HI 21 cm are important because the gas component in a galactic disk extends further than the stellar component, beyond the optical boundaries. But García-Ruiz, Sancisi and Kuijken (2002) argue that a optical+HI study of warps could bring important information about on the mechanisms that lead to the formation of warps.

The warp of the Milky Way is known since the 1950s (BURKE, 1957; KERR, 1957). With more robust mapping surveys, it is possible to perform more detailed investigations into the structure of our galaxy. Recent studies have provided more insights into the aspects of the Galactic warp based on observational data (e.g. HUANG *et al.*, 2018; SCHÖNRICH; DEHNEN, 2018; ROMERO-GÓMEZ *et al.*, 2019; CHENG *et al.*, 2020; CHROBÁKOVÁ; NAGY; LÓPEZ-CORREDOIRA, 2020; POGGIO *et al.*, 2020; DEHNEN; SEMCZUK; SCHÖNRICH, 2023) and also on simulations (e.g. LAPORTE *et al.*, 2018; POGGIO *et al.*, 2021; BLAND-HAWTHORN; TEPPER-GARCÍA, 2021). Using Cepheids as tracers, Dehnen, Semczuk and Schönrich (2023) found a warp signal reaching an inclination of $i \sim 3$ °at $R \geq 14$ kpc. Other investigations showed that the Galactic warp is twisted (e.g. ROMERO-GÓMEZ *et al.*, 2019) and has a larger amplitude on one side (CHROBÁKOVÁ; NAGY; LÓPEZ-CORREDOIRA, 2020). The origin of the Galactic warp is still under debate, but many of these works point out that the interaction with the Sagittarius dwarf galaxy probably causes the bending waves in the Milky Way.

Because of the challenges of observational studies on warps, simulations can be a very useful instrument to understand the evolution of vertical perturbations and their properties, such as duration, amplitude and, most importantly, the mechanisms that can trigger warp formation. Some of these mechanisms are accretion of misaligned cold gas in the galactic disk (GÓMEZ *et al.*, 2017; KHACHATURYANTS *et al.*, 2022), misalignment between the stellar disk and the inner dark matter halo (HAN *et al.*, 2023; GARCÍA-CONDE *et al.*, 2024), and even more subtle factors, such as misalignment between the angular momentum and the angular velocity in models of barred galaxies (SÁNCHEZ-MARTÍN; ROMERO-GÓMEZ; MASDEMONT, 2016) or random noise in the distribution of halo and bulge particles in N-body simulations (CHEQUERS; WIDROW, 2017). In addition, the role of external perturbations (fly-bys and interactions with satellites) is reinforced by many studies (e.g. GÓMEZ *et al.*, 2017; SEMCZUK *et al.*, 2020; TEPPER-GARCÍA; BLAND-HAWTHORN; LI, 2020; TEPPER-GARCÍA; BLAND-HAWTHORN; FREEMAN, 2022; GARCÍA-CONDE *et al.*, 2024). Despite all the other possibilities, tidal interactions seem to be the most obvious mechanism that induces features in the outer disk. Furthermore, as the phenomena mentioned above induce mainly S-shaped warps, it has been suggested that U-shaped warps can be formed by another mechanism: ram pressure stripping (ZEE *et al.*, 2022).

There are also different methods for characterizing the warp intensity. Some studies define a warp starting radius, where the disk begins to tilt significantly towards its innermost part. With this parameter, it is possible to determine the warp angle or inclination (e.g. GARCÍA-RUIZ; SANCISI; KUIJKEN, 2002; SEMCZUK *et al.*, 2020) or the amplitude of the warp with respect to the galactic radius (e.g. POGGIO *et al.*, 2017; POGGIO *et al.*, 2020). Another method for measuring asymmetric features, such as warps and lopsidedness, is to use the amplitude of the $m = 1$ Fourier mode (e.g. POGGIO *et al.*, 2021; VARELA-LAVIN *et al.*, 2023).

1.5 AIMS

Warps and bars are common features, appearing in more than half of spiral galaxies, including the Milky Way, as shown by the studies cited in sections 1.2 and 1.3. Several investigations also point out that satellites may have an influence on the development of both structures. But there are still not many investigations that specifically explore the formation of warps in barred galaxies. In this study, we aim to understand if a barred galaxy is more resilient against warping, or more susceptible to it, compared to a galaxy that does not have a bar. We used N-body simulations of galaxies interacting with satellites of varying masses and initial orbital radii to analyze the effects of warps induced by these satellites on barred and non-barred galaxies.

This study is organized as follows: in chapter 2 describe the details of the simulation setup and the characteristics of central galaxies and satellites; chapter 3 presents the results of the interactions and analysis about bar aspects and warp development, as well as a discussion with comparisons with other studies; and chapter 4 contains the conclusions. The appendix shows additional analyses of the topics discussed in the chapters.

2 METHODS

This chapter presents, in the first section, some aspects of N-body simulations used in astronomy and the code used to run the simulations in this study. Then, in the following two sections, the initial conditions of the models and their parameters are detailed. Our models are composed of a massive central galaxy, and a satellite galaxy orbiting it. The central galaxy can be barred or non-barred and the satellites can have different masses and initial orbital radii.

2.1 N-BODY SIMULATIONS

As mentioned in the introduction (chapter 1), computational simulations are widely used in extragalactic astronomy (and other fields). In general, these simulations are mathematical models performed by computers that aim to describe a real system. They are important for understanding specific aspects of a phenomenon and for making predictions. For astronomy, this is very relevant, as the scales of time and space are very large, there is a limitation in understanding the real evolution of various objects and phenomena. In simulations, galaxies can be represented by a group of N-particles (bodies) that interact gravitationally with each other, as shown in Figure 5. An interaction between two bodies has an analytical solution, with Newtonian dynamics equations. However, the problem for 3 or more interacting bodies is only solved numerically.

Figure 5 – Group of bodies interacting.

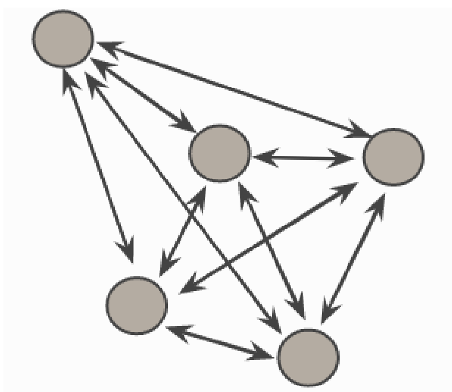

Source: The author (2024).

Over the years, codes have been developed to represent gravitational systems. The first codes ran isolated galaxies to analyse, for example, the formation of the bar and spiral arms (HOHL, 1971; OSTRIKER; PEEBLES, 1973; PATSIS; KAUFMANN, 1999). These local simulations had improvements and are also often used today. They are important to represent the evolution of a simple system in detail. Later, cosmological simulations were developed, with a much larger volume of data. They calculate the evolution of the components of the universe and are useful tools for understanding the formation of large scale structure. Examples of codes used in cosmological simulations are the GADGET (GAlaxies with Dark matter and Gas intEracT) code, used in the Millennium Run simulation (SPRINGEL *et al.*, 2005) and in the Eagle Project (SCHAYE *et al.*, 2015), and the AREPO code (SPRINGEL, 2010), used in the Illustris Project (GENEL *et al.*, 2014). Many codes can run both local and cosmological simulations, and they can perform N-body simulations, with particles that represent dark matter and stars interacting only gravitationally, or they can include hydrodynamics to represent gas interactions.

Studies using simulations can be divided into three stages: creating initial conditions for the system to be studied; running the simulation; and analyzing specific aspects of the outputs. We used the galstep code (RUGGIERO; NETO, 2017) to create the initial conditions and the GADGET-4 code (SPRINGEL *et al.*, 2021) to run local simulations. These codes use different types of particles to represent the components of the galaxy: halo, disk, bulge, gas and stars. The halo particles represent the dark matter. The rest represents baryonic matter. The disk and bulge particles are the stars in the disk and in the bulge regions, and they are represented by separate particles because their distribution is different. The gas particles are in the disk and give rise to new stars as the simulation progresses, via cooling and star formation. Finally, stars particles are these new stars that come from gas. Unlike disk particles, they are not present in the initial conditions and the number of particles are not constant (it increases as the gas is consumed).

It is important to note that simulations in this study are idealised and do not distinguish between thin and thick disks, do not have chemical information about stellar populations (like the AREPO code, for example), among other factors. The models are isolated, they are not part of an environment such as a group or a cluster.

The GADGET code performs N-body simulations with the Barnes and Hut (1986) oct-tree structure, a kind of tree algorithm (APPEL, 1985) which hierarchically organize the particles in groups and calculate the gravitational field at a given point considering those groups. The halo, disk, bulge and stars particles interact according to this method. However, the interaction of gas particles is best performed using other approach. GADGET uses SPH (Smoothed-Particle Hydrodynamics) (GINGOLD; MONAGHAN, 1977; LUCY, 1977), which considers interpolations with the neighbor particles to define positions.

2.2 CENTRAL GALAXIES

Our first central galaxy model is spiral galaxy with a strong bar (hereafter referred to as "model B"). It is composed of a disk, a bulge and a dark matter halo. The disk density profile is given by equation (1):

$$\rho(R, z) = \frac{M_{\rm d}}{4\pi R_0^2 z_0} \exp\left(\frac{-R}{R_0}\right) \operatorname{sech}^2\left(\frac{z}{z_0}\right), \tag{1}$$

where the disk mass is $M_{\rm d} = 4 \times 10^{10} {\rm M}_\odot$, the radial scale length is $R_0 = 3.5$ kpc and the vertical scale length is $z_0 = 0.7$ kpc. For the halo, we used the Hernquist (1990) profile, given by equation (2):

$$\rho(r) = \frac{M_{\rm h}}{2\pi} \frac{a}{r} \frac{1}{(r + a)^3}, \tag{2}$$

where the scale length is $a = 47$ kpc and the halo mass is $M_{\rm h} = 1 \times 10^{12} {\rm M}_\odot$. Finally, the bulge follows the same density profile, but with a smaller scale length, $a = 1.5$ kpc. It has a mass of $M_{\rm b} = 1 \times 10^{10} {\rm M}_\odot$, i.e. it corresponds to 20 per cent of the total baryonic mass. The scale length values used are meant to approximate a Milky Way-like galaxy. Figure 6 shows the circular velocity curves for each component of the galaxy (disk, halo and bulge), as well as the total curve, which is flat because of the large amount of dark matter present in the galaxy, as already explained in section 1.2. The circular velocity v_c is calculated considering the mass M contained within each radius r, according to equation 3:

$$v_c = \sqrt{\frac{GM(r)}{r}} \tag{3}$$

We used the galstep code (RUGGIERO; NETO, 2017) to create the initial conditions, setting the masses mentioned above and an appropriate number of particles for each component. They are chosen taking into account the desired resolution and computational cost. The disk has $N_{\rm d} = 2 \times 10^5$ particles, the bulge has $N_{\rm b} = 0.5 \times 10^5$ particles, and the halo has $N_{\rm h} = 1 \times 10^6$ particles. After establishing the initial conditions, we used the GADGET-4 code (SPRINGEL *et al.*, 2021) to run the simulations. To prevent large-angle scatterings and avoid the formation of pairs of bound particles, the code uses a smoothing parameter: the gravitational softening length ϵ. The optimal gravitational softening length in principle depends on the number of particles and the size of the system. We used 0.1 kpc for all the components.

Figure 6 – Circular velocity curve of the barred galaxy.

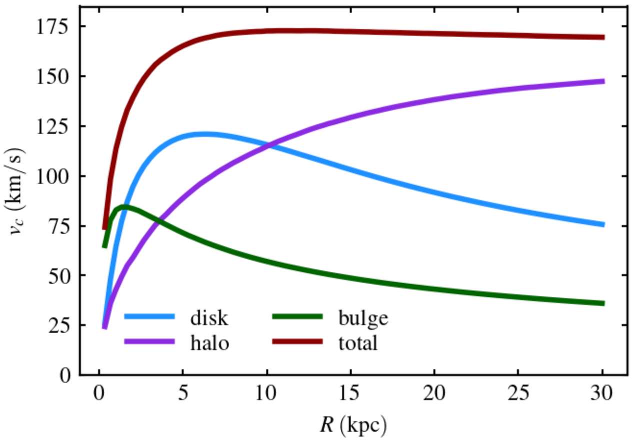

Source: The author (2024).

In the analysis of galactic bars in N-body simulations, it is usually sufficient for the galaxy to evolve for a few gigayears. However, in this study, we need to extend the simulation longer. The introduction of satellites must happen when the bar in the central galaxy is already well-developed and robust, and then, the interaction between the two galaxies must last a few more Gyr to be effective. For this reason, we let the model evolve for a total 14 Gyr, saving outputs every 0.05 Gyr.

For comparison in future analyses, we need a second model, a galaxy with the same size and mass, but non-barred. Bars appear spontaneously in a large number of studies with N-body simulations (ATHANASSOULA; MISIRIOTIS, 2002), but the presence of gas in the disk is known to inhibit the formation of strong bars in simulated galaxies (ATHANASSOULA; MACHADO; RODIONOV, 2013). Then, this model is a non-barred spiral galaxy (hereafter referred to as “model NB”), with disk, bulge, gas and dark matter halo. The initial conditions were also created with the galstep code, but some parameters have changed. The extra component in this model, the gas, also has an exponential density profile described by equation (1), but with $z_0 = 0.035$ kpc. The other components follow the same density profiles shown in equations (1) (disk) and (2) (halo and bulge). The halo mass is also $M_h = 1 \times 10^{12} M_\odot$ and the baryonic mass is still $5 \times 10^{10} M_\odot$. But, because of the gas addition, the baryonic mass was distributed differently from model B: here, the gas represents initially 75 per cent of the baryonic mass, hence $M_g = 3.75 \times 10^{10} M_\odot$. The rest ($1.25 \times 10^{10} M_\odot$) was distributed between disk and bulge. The bulge has 20 per cent of this mass, resulting in $M_b = 0.25 \times 10^{10}\, M_\odot$, and the disk mass is $M_d = 1 \times 10^{10}\, M_\odot$.

The initial conditions of model NB were relaxed in isolation for 4.2 Gyr without star formation, to allow numerical transients time to dissipate. After that, the definitive simulation ran with the same time evolution as model B, now including cooling and star formation. We used the same gravitational softening length and the outputs were also saved every 0.05 Gyr.

At the end of the simulations, the presence or absence of gas in the galactic disk resulted in models B and NB having very different morphologies. Figure 7 shows the final face-on and edge-on projections of the galaxies. Our first model ended up being a strongly barred galaxy with a peanut-shaped bar, and the second model is a galaxy that does not develop a bar, maintaining a more axisymmetric shape.

In order to quantify this difference in the central part of the galaxies, we calculated the bar strength A_2 for each one. We used the maximum value of the relative amplitude of the $m = 2$ mode of the projected mass distribution (ATHANASSOULA; MACHADO; RODIONOV, 2013; ŁOKAS, 2019a; PESCHKEN; ŁOKAS, 2018; CUOMO *et al.*, 2019). This mode is sensitive to non-axisymmetric configurations, which is the case for an elongated structure like the bar. A_2 is given by equation (4):

$$A_2 = \max\left(\frac{\sqrt{a_2^2 + b_2^2}}{a_0}\right), \tag{4}$$

where a_m and b_m are the Fourier coefficients shown by equations (5) and (6):

$$a_m(R) = \sum_{i=0}^{N_R} m_i \cos(m\,\theta_i),\ m = 0{,}1{,}2... \tag{5}$$

$$b_m(R) = \sum_{i=0}^{N_R} m_i \,\mathrm{sen}(m\,\theta_i),\ m = 1{,}2... \tag{6}$$

with m_i being the mass in each ring i of radius R.

Figure 8 shows the time evolution of A_2 for the two models. As expected, the barred galaxy has a much higher final A_2 value than the non-barred galaxy. It has four clear phases: rapid growth, an almost flat phase, a sudden decrease (buckling), and a smooth secular evolution. Buckling is characterized by vertical instabilities in the bar that weaken it for a short period (e.g. ŁOKAS, 2019b; ŁOKAS, 2019a). It is possible to quantify the loss of symmetry in the bar calculating the difference S between the A_2 of the particles above the $z = 0$ plane of the disc and the A_2 of the particles below this plane, as shown in equation (7):

Figure 7 – Morphology of the galaxies at the end of the simulation (14 Gyr). On the left, the barred galaxy (model B), seen face-on in the top panel and edge-on in the bottom panel. On the right, the non-barred galaxy (model NB), also seen in the face-on and edge-on projections.

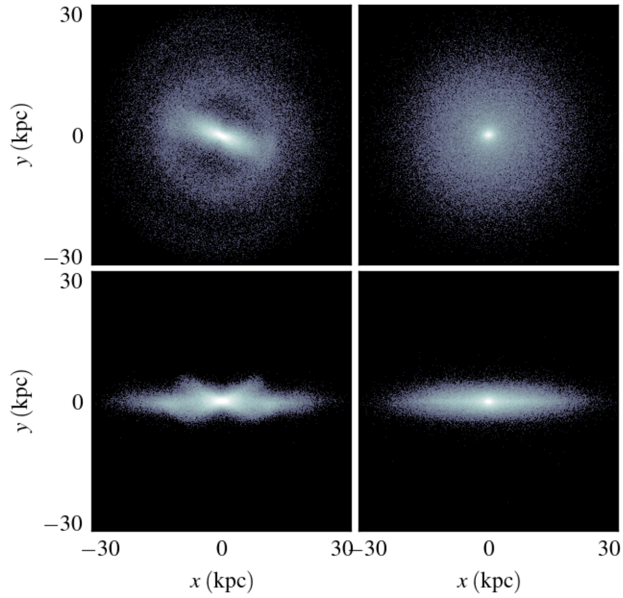

Source: The author (2024).

$$S = |A_2(z > 0) - A_2(z < 0)|. \tag{7}$$

At all times, this difference will be almost zero, except at the moment of buckling. Figure 9 shows the evolution of S. Its peak occurs at $t = 3.2$ Gyr and the morphology of the bar region at this moment is illustrated in Figure 10.

Figure 8 – Evolution of bar strength A_2. The black points mark the moment when the satellite galaxies are added to the simulation, at $t = 8$ Gyr.

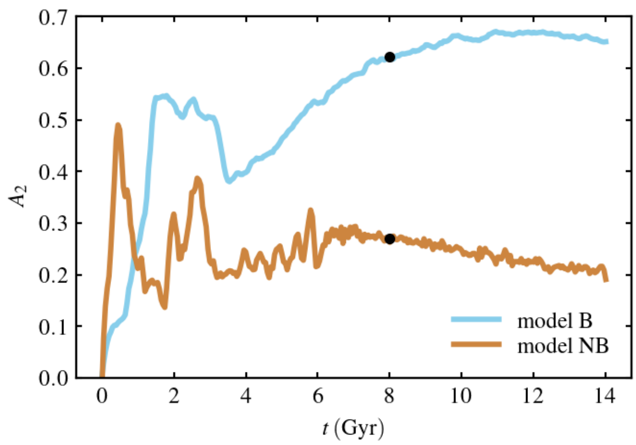

Source: The author (2024).

Figure 9 – Evolution of bar asymmetry S.

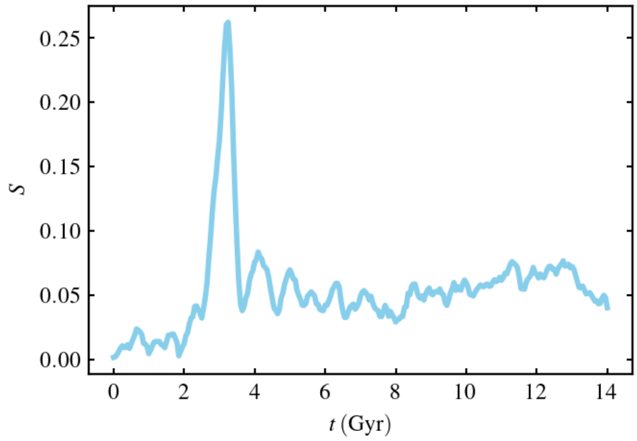

Source: The author (2024).

Figure 10 – Edge-on morphology of the bar at $t = 3.2$ Gyr due to buckling, which leads to a difference in shape between the parts above and below the $z = 0$ plane, as evidenced by the white line.

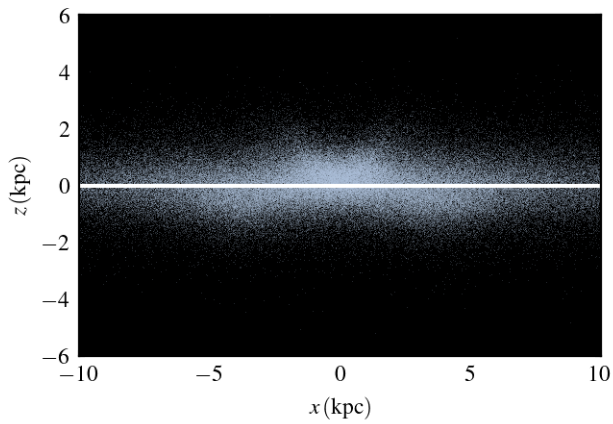

Source: The author (2024).

In Figure 8, the non-barred galaxy, despite ending up with low A_2 values, shows some peaks at the beginning of the simulation. We verified that this does not indicate the formation of a bar, but only transient asymmetries in the central part of the disk. It also can be noted that the bar is already very robust in model B and that there are no instabilities in model NB at $t = 8$ Gyr, the time chosen for the satellite galaxies to be introduced into the simulations to orbit the central galaxies.

2.3 SATELLITE GALAXIES

The initial conditions of the satellites were created with the Hernquist density profile defined in equation (2). The scale length is $a = 0.4$ kpc and the masses are $0.1 \times 10^{10} \mathrm{M}_{\odot}$,

$0.5 \times 10^{10} M_\odot$ and $1 \times 10^{10} M_\odot$, which represents, respectively, 2, 10 and 20 per cent of the baryonic mass of the central galaxy that the satellites will orbit. These three masses were labeled as M1, M2 and M3. The effect of the satellites on the host galaxy depends mainly on their mass, not on their internal structure. Since dark matter is the predominant component of the total mass, we created the initial conditions with dark matter only. We have verified that satellites built this way are stable if they evolve in isolation.

The satellite galaxies are spherical and were positioned in polar orbits around to the central galaxy, as shown in Figure 11. The initial radii of the satellites are 10 kpc, 20 kpc and 30 kpc. These radii were labeled as R1, R2 and R3. All the orbits are initially circular and last from 8 to 14 Gyr. The initial velocities of the satellites are the circular velocities corresponding to each radius: 165 $km\,s^{-1}$, 171 $km\,s^{-1}$ and 169 $km\,s^{-1}$ for radii R1, R2 and R3, respectively. These velocities were established based on the velocity curves of the central galaxies, to ensure that the orbit is initially circular. As the rotation curve of the central galaxies (Figure 6) is approximately flat in the 10 – 30 kpc radial range, it is natural that these velocities are similar to each other. Figures 12 and 13 show each of the 9 models around galaxy B, and then again around galaxy NB. Note that in all cases, the satellite galaxy ends up absorbed, except in models M1R3 and M1R2, where the simulation ends without merging. At each time step, the position of the satellite galaxy was determined using the density peak of its particles. In cases where the satellite has been absorbed by the central galaxy, this peak is not well defined, as the satellite has already lost many of its particles.

Since the central galaxies can have different morphologies and the satellites can have different masses and orbital radii, Table 1 summarizes the main information about these variables and identifies each model. For each of the 3 masses of the satellite galaxy, we have 3 orbital radii. Therefore, we have 9 models around galaxy B, and another 9 models around galaxy NB, resulting in a total of 18 simulations. There are also the models B and NB that have been continued in isolation. Each one will have the central part and edges of the disk affected differently, depending on the combination of the parameters.

Figure 11 – Example of central galaxy and satellite (model NB-M3R2).

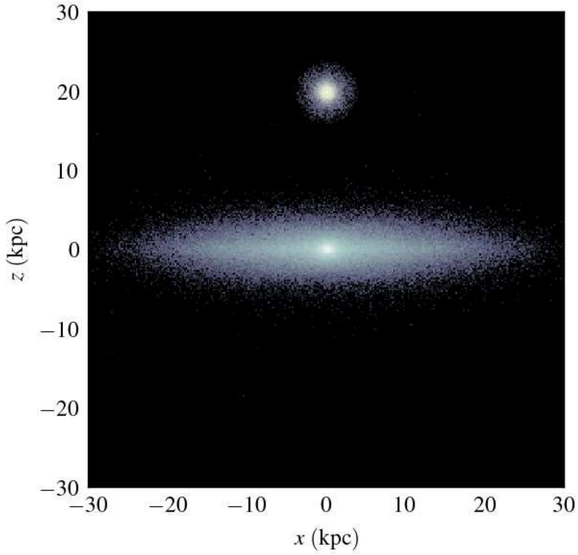

Source: The author (2024).

Figure 12 – Satellite orbits around the barred galaxy during 6 Gyr (from 8 to 14 Gyr). From left to right, the masses of the satellites increase ($0.1 \times 10^{10}M_\odot$ (M1), $0.5 \times 10^{10}M_\odot$ (M2) and $1 \times 10^{10}M_\odot$ (M3)), and from top to bottom, the orbital radii decrease (30 kpc (R3), 20 kpc (R2) and 10 kpc (R1)). Thus, the yellowish tones characterize the lower mass satellites, the green tones characterize the intermediate mass satellites, and the purple tones the higher mass satellites. Light shades represent smaller radii, and darker shades represent larger radii.

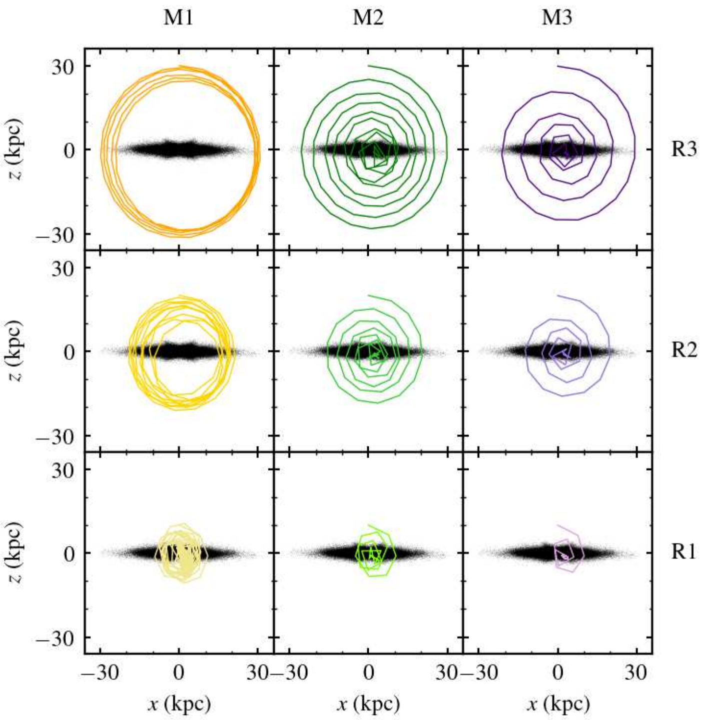

Source: The author (2024).

Figure 13 – Satellite orbits around the non-barred galaxy during 6 Gyr. The color scheme is the same as in Figure 12.

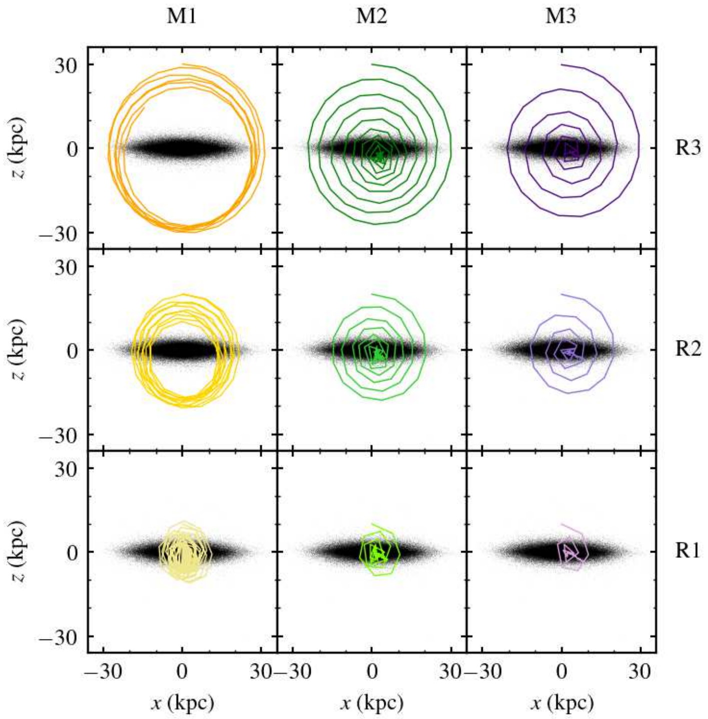

Source: The author (2024).

Table 1 – Names and parameters for each model.

Model name	Central galaxy	Satellite mass ($10^{10}M_\odot$)	Satellite initial radius (kpc)
B-M1R1	Barred	0.1	10
B-M2R1	Barred	0.5	10
B-M3R1	Barred	1	10
B-M1R2	Barred	0.1	20
B-M2R2	Barred	0.5	20
B-M3R2	Barred	1	20
B-M1R3	Barred	0.1	30
B-M2R3	Barred	0.5	30
B-M3R3	Barred	1	30
NB-M1R1	Non-barred	0.1	10
NB-M2R1	Non-barred	0.5	10
NB-M3R1	Non-barred	1	10
NB-M1R2	Non-barred	0.1	20
NB-M2R2	Non-barred	0.5	20
NB-M3R2	Non-barred	1	20
NB-M1R3	Non-barred	0.1	30
NB-M2R3	Non-barred	0.5	30
NB-M3R3	Non-barred	1	30

3 RESULTS

In this section, we show the main results of our investigations. The first section focuses on the analysis of how the different satellite models affect the bar development in the barred galaxy. In the second section, we show the influence of the satellite on the occurrence of warps and we compare the intensity of this phenomenon in the barred and non-barred galaxies. Then, in the third section, we present a test to check the reliability of our results on the difference in warp intensity in models B and NB. Finally, the last section discusses the results obtained and compares them with other studies.

3.1 HOW THE PERTUBER AFFECTS BAR STRENGTH

The close passage of the satellites caused changes in the strength and the shape of the bar in model B. To quantify these changes, we calculated A_2 (equation (4)) for all the perturbed models to compare it with the isolated one. In Figure 14 it is evident that bar strength decrease is directly related to the mass and orbit of the satellite. The mass influences in how much the bar will lose strength: less massive perturbers (M1) barely affect A_2, and the bar remain as strong as in the isolated B model; satellites of intermediate mass (M2) weaken the bar without destroying it; and the most massive satellites (M3) destroy the bar, as evidenced by the large decline in A_2 values. In addition to the mass, another parameter of the perturber is relevant: the satellite's orbital radius determines the moment where strength decrease will occur. For satellites with masses M2 and M3, it is noticeable in Figure 14 that the closer the satellite's orbit, the sooner the bar is attenuated or destroyed, compared to more distant orbits. Therefore, the changes in A_2 occur first for satellites with initial orbital radius R1, then R2 and finally R3. We did the same analysis for the non-barred galaxy. As the focus of this section is the barred galaxy, the corresponding figure for model NB is presented in the appendix, in the section A.1.

Figure 15 shows the change in the shape of the bar. The central galaxy (model B) is seen face-on after the interaction with the satellite, at $t = 14$ Gyr. Each combination of parameters results in different final bar shapes, that can be perceived based on visual inspection. The interaction with the low-mass satellites (M1) does not affect its rectangular shape; satellites of intermediate mass (M2) weaken the bar, leaving it smaller and with a mildly oval shape; and finally, the merger with the most massive satellites (M3) cause destruction of the bar, leaving the

Figure 14 – Evolution of bar strength in isolated and perturbed models of the barred galaxy. Again, the color scheme is the same as in Figure 12.

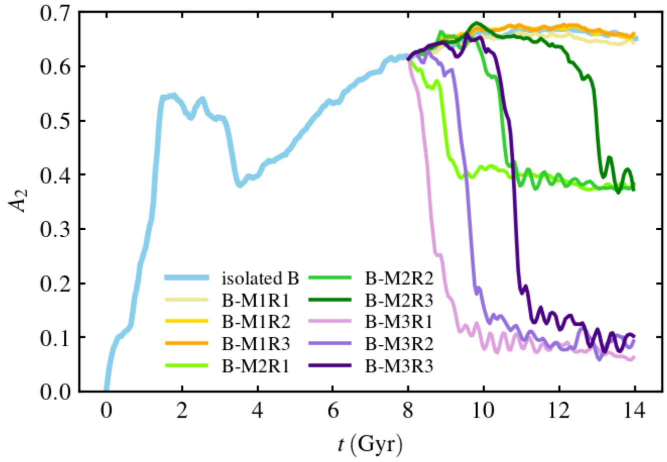

Source: The author (2024).

disk configuration axisymmetric. This visualization confirms the results of Figure 14. The mass of the satellite is an impacting factor on the decrease in bar strength: shorter, rounder bars are weaker (lower A_2) and longer, rectangular bars are stronger (higher A_2). Here the initial orbital radii of the satellites make no difference because the chosen time is the end of the simulation and all the interactions have already occurred. The final A_2 only depends on the mass of the satellite: regardless of the orbital radius, the A_2 values for a given mass M are very close. As we have seen, the orbital radius of the perturber has an impact on the moment of the reduction in the bar strength, but it occurs before the end of the simulation in all cases.

Since the initial radius of the orbit determines whether the decline in bar strength will happen earlier or later, we also analyzed the evolution of the satellite's orbital radius r together with the evolution of the bar strength A_2 in the central galaxy. Figure 16 shows one example (for model B-M2R2) of the temporal correlation between the greater proximity of the satellite and lower A_2 values. These results apply to all other simulations with intermediate (M2) and massive (M3) satellites as well. These figures are in the appendix, in the section A.2.

3.2 DEVELOPMENT OF THE WARPS

The formation of warps has also been noted during the interaction between the central galaxies and the satellites: an example is shown in Figure 17. We initially studied maps of mean heights z in order to qualitatively characterize the differences between the models. Figure 18 shows an example of a mean heights map for model B-M3R1 at 3 selected times. The warp

Figure 15 – Face-on barred galaxy showing the impact of the satellites on the shape of the galactic bar.

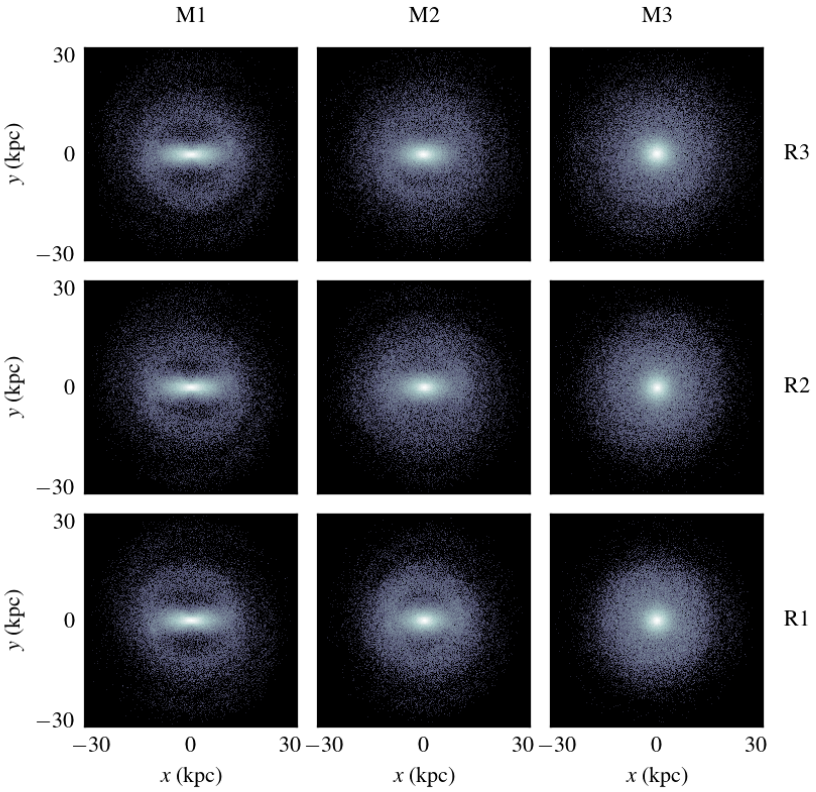

Source: The author (2024).

Figure 16 – Evolution of the satellite's orbital radius r together with the evolution of the bar strength A_2 in the central galaxy for model B-M2R2. Note the different axes for each variable. As the satellite approaches the center of the galaxy, the bar strength decreases.

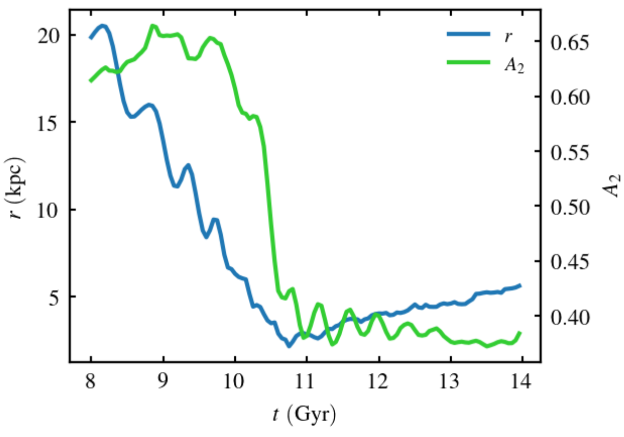

Source: The author (2024).

evolves over time in a spiral appearance, and to keep all the panels in the same orientation, we rotated the disk so that the bar (although it doesn't appear in the figure) coincides with the x-axis. At $t = 8$ Gyr, the disk of the central galaxy has mean heights close to zero, indicating that the disk is initially symmetric with respect to the $z = 0$ plane, but within a few Gyr, the edges of the disk are deformed by the gravitational influence of the satellite, and one part is bent upwards and the other downwards, characterizing the S-shaped warp. There is also a certain asymmetry in the central part of the disk, but with less intensity. This morphology is preserved until the end of the simulation. The process is similar for the other models, which are shown in section A.3 of the appendix.

Figure 17 – Warp in the model B-M3R1 at $t = 13$ Gyr.

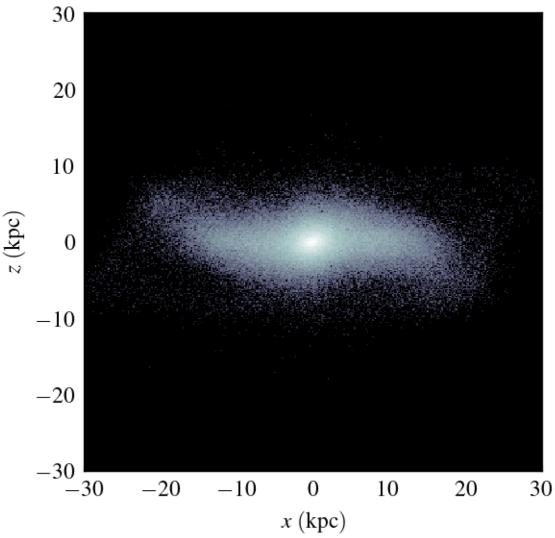

Source: The author (2024).

Figure 18 – Mean heights map for model B-M3R1 at different times, showing the difference in the heights z of the edge of the galactic disk after interaction with the satellite.

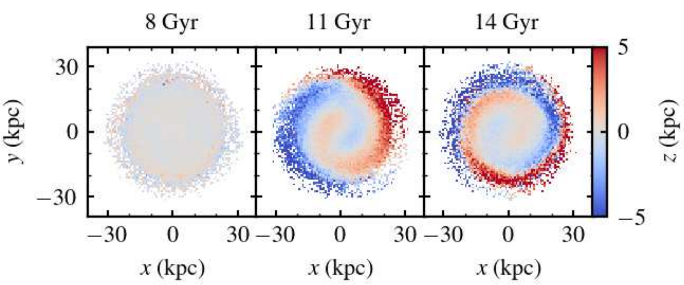

Source: The author (2024).

When comparing barred and non-barred galaxies, we noted differences in the intensities of the warps induced by the same satellite. Figure 19 presents the morphologies of the galaxies at

$t = 14$ Gyr considering the isolated cases and the interaction with a satellite of mass $1 \times 10^{10} M_{\odot}$ and orbital radius 30 kpc. For the barred galaxy, the bar has been rotated to coincide with the x-axis, but this is only noticeable in the top panel, where the range of z is smaller. In the bottom panel, the range is larger, and at the time shown, the bar has already been destroyed by interaction with the most massive satellite. There is no clear warp signal in the isolated cases (top panel), but in the perturbed ones (bottom panel), the barred galaxy exhibits a more intense warp than the non-barred galaxy. This pattern was also found in all the other models, as shown in Figures 20 and 21.

Figure 19 – Top panel: map of mean heights for models B and NB (isolated) at $t = 14$ Gyr. In model B, the bar can be seen in the center. Bottom panel: map of mean heights for models B-M3R3 and NB-M3R3 at $t = 14$ Gyr. Note the different ranges in the colorbars.

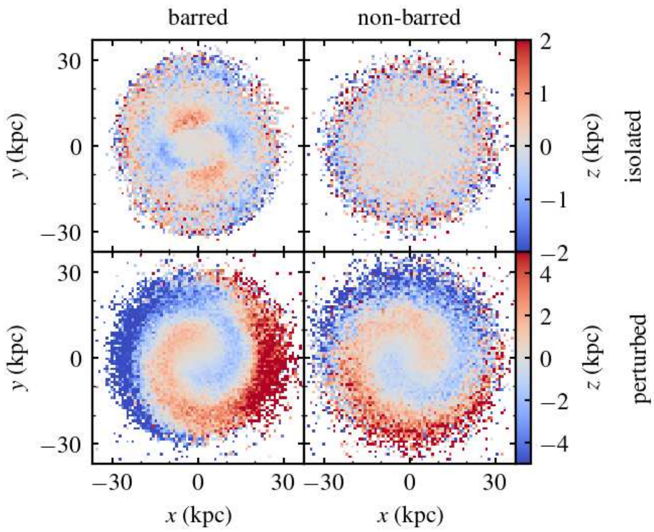

Source: The author (2024).

Figures 20 and 21 show the mean heights maps for barred galaxy and non-barred galaxy. As in figures above, the bar has been rotated in the B models. Comparing each NB panel with its equivalent in B, it is clear that the intensity of the induced warp is greater in the barred galaxy in each case, even in cases where the satellite does not merge with the central galaxy (models M1R2 and M1R3, see Figures 12 and 13). There is also an indication that the intensity depends essentially on the mass of the perturber, for both B and NB galaxies. The lowest mass satellites (M1) cause very small asymmetries in the outer disk of the central galaxies, and the larger mass satellites (M2 and M3) induce more pronounced warps, with the strongest ones resulting from from the perturbation of satellites with mass M3. So for each orbital radius R, the warp intensity increases systematically with the mass M. On the other hand, for a given M, the warp intensity is not clearly correlated with R.

Figure 20 – Map of mean heights at t = 14 Gyr for all models of perturbed barred galaxy. As in Figures 12 and 15, from left to right, the masses of the satellites increase, and from top to bottom, the orbital radii decrease.

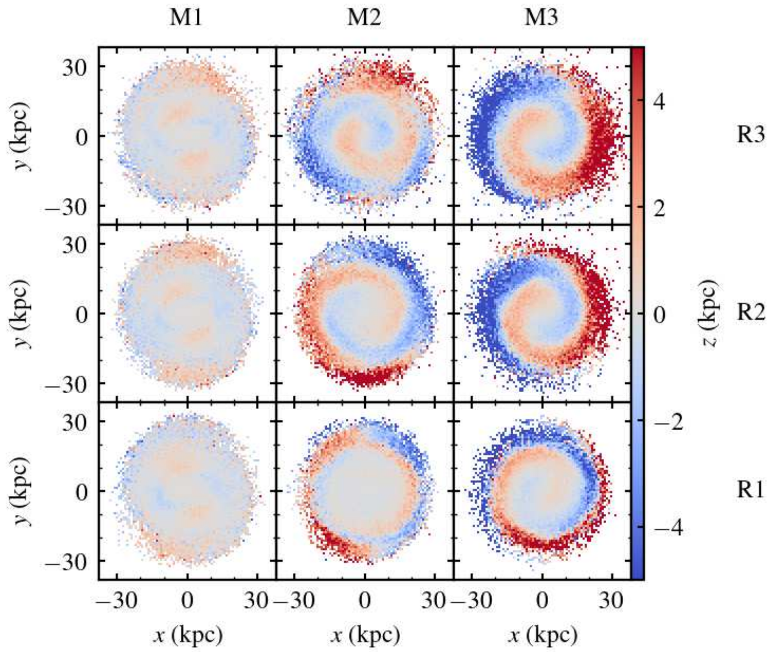

Source: The author (2024).

Figure 21 – Map of mean heights at t = 14 Gyr for all models of perturbed non-barred galaxy.

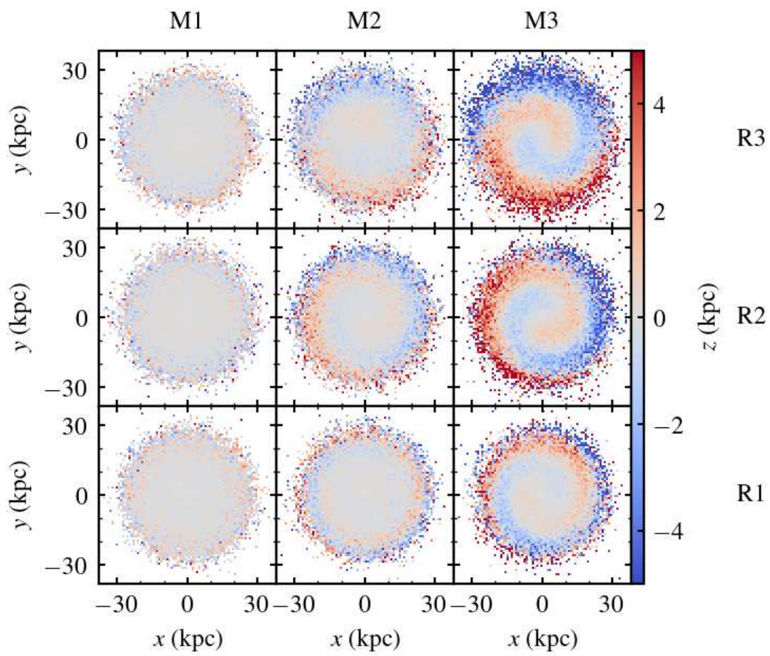

Source: The author (2024).

Once these differences between B and NB models were noted, we performed a quantitative analysis of the warp intensity using two methods. In the first, we considered the time evolution of heights z as a function of the azimuthal angle θ in the xy plane. This analysis was carried out in an outer ring of the disk ($20 < R < 30$ kpc, where R is the cylindrical radius). Figure 22 shows an example for model B-M3R1 at 3 selected times (same model and selected times as Figure 18). At each instant of time, there is a maximum and a minimum value of z, which characterize, respectively, the part of the edge of the disk that is tilted upwards and the part that is tilted downwards. The maximum amplitude of the warp W is defined by equation (8):

$$W(t) = \frac{z_{\max} + |z_{\min}|}{2}. \tag{8}$$

The evolution of W is shown in Figure 23 for the interacting models. To ensure that the results of this measurement do not depend strongly on the choice of ring, we also tested with a more internal ring ($10 < R < 20$ kpc), which displays the same pattern and is shown in section A.4 in the appendix. Figure 23 supports what the mean height maps indicated: the warp is more intense in the barred galaxy in all cases, regardless of the perturbation, and the amplitude of the warp depends on the mass of the perturber. The orbital radius of the satellite does not seem to be a decisive factor.

If there is such a difference of intensity in the perturbed models, it is reasonable to question if the barred galaxy would have an intrinsic tendency to develop more intense warps even in isolation. In Figure 24, we have the evolution of W for the isolated models. We used the same amplitude range as in Figure 23 for comparison. During most of the simulation, there is almost no disparity in the values of W in the B and NB galaxies, but at approximately 10 Gyr, a small warp signal in the barred galaxy appears without any disturbance. The inset in Figure 24 highlights this increase in W in the barred galaxy, while the value remains almost constant in the non-barred galaxy.

The second method for measuring the vertical distortions is calculating A_1, using Fourier components a_1 and b_1, corresponding to the $m = 1$ mode, according to the equations (9) and (10):

$$a_m(R) = \frac{1}{N_R} \sum_{i=0}^{N_R} z_i \cos(m\,\theta_i),\ m = 0,1,2... \tag{9}$$

$$b_m(R) = \frac{1}{N_R} \sum_{i=0}^{N_R} z_i \,\mathrm{sen}(m\,\theta_i),\ m = 1,2... \tag{10}$$

Figure 22 – Mean heights as a function of the azimuthal angle θ for model B-M3R1 at 3 selected times.

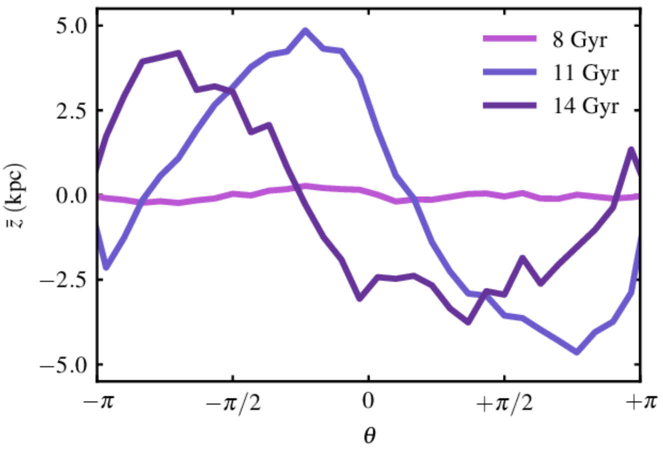

Source: The author (2024).

Figure 23 – Evolution of maximum amplitude of warp W for all perturbed models.

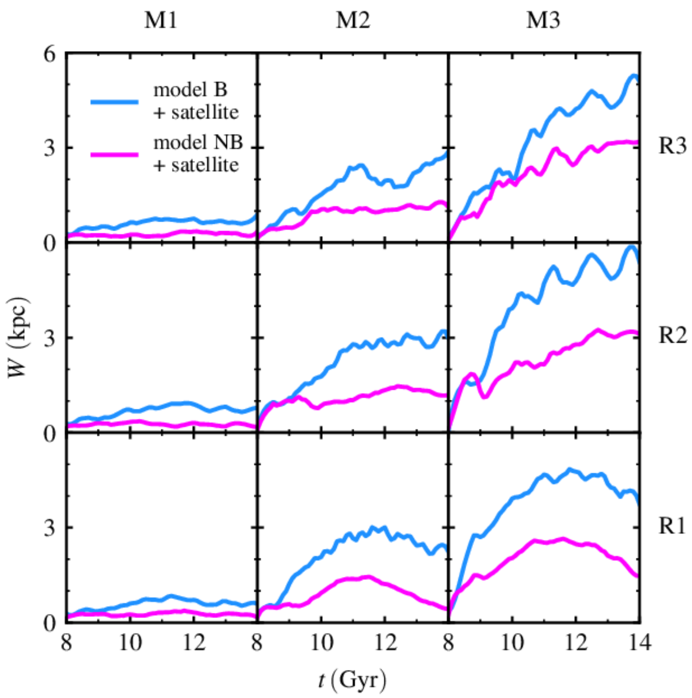

Source: The author (2024).

Figure 24 – Evolution of maximum amplitude of warp W for isolated models B and NB.

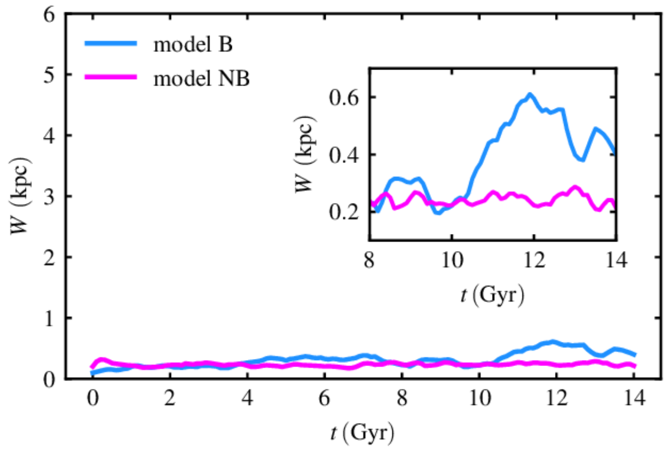

Source: The author (2024).

where z_i is the height in each ring i of radius R and N_R is the number of particles in each ring. Then, A_1 is given by equation (11):

$$A_1 = \sqrt{a_1^2 + b_1^2}. \tag{11}$$

The quantity A_1 defined in this way acts as a measure of the intensity of the bending mode (e.g. GARCÍA-CONDE *et al.*; 2024). Figures 25 and 26 show A_1 for the perturbed models of barred and non-barred galaxies. The lighter, yellowish colors mark the areas where the warp is most intense. There is a predominance of these colors in the outermost radii of the disk in cases where the central galaxies are perturbed by the satellites of mass M2 and M3. Again, it can be noted the difference in the warp induced in the barred and non-barred galaxies, as well as the influence of the mass of the satellite on the intensity of this distortion. Figure 27 shows A_1 for the isolated cases. Even without disturbances, in model B it is possible to see lighter regions in the larger radii, something that does not happen in model NB. One of these lighter regions is an intrinsic warp signal that can be related to the peak of W around 12 Gyr, seen in the inset of Figure 24.

In Figure 25, it is also possible to identify that the maximum intensity of the warp (very yellow regions) is reached after 10 Gyr. The greenish and light blue areas appearing in the inner regions of the disk ($0 < R < 20$ kpc) indicate that the asymmetry appears also in the central region, but with less intensity. The time it takes depends on the orbital radius of the satellite: when the satellite has a smaller orbit (R1), the distortions in the center and at the edges occur at the same time, at the start of the simulation. But for the satellite with larger radius (R3), the warp is first established on the edges of the disk and only after a few Gyr it also appears in the central regions.

Figure 25 – A_1 for all perturbed models of the barred galaxy. Note the different ranges in the colorbars.

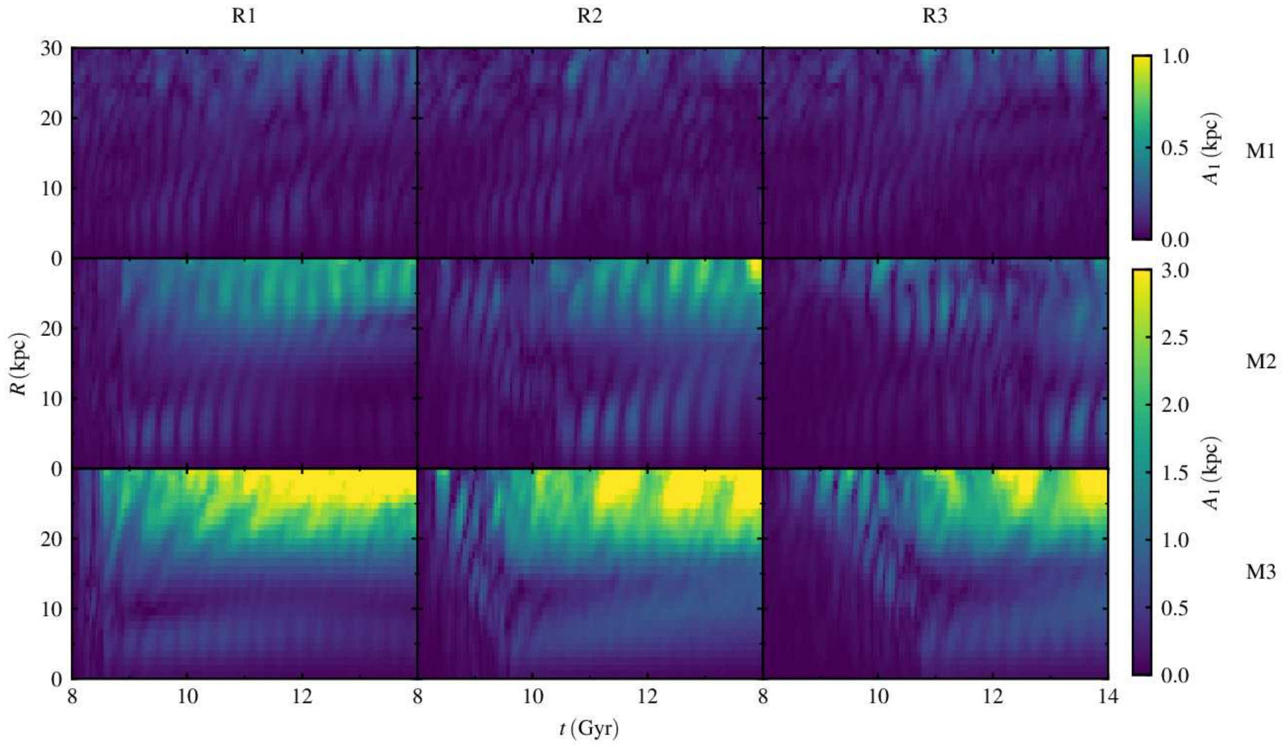

Source: The author (2024).

Finally, Figures 28 and 29 show the disks seen edge-on and the appearance of the warps induced in the barred and non-barred galaxies at $t = 13$ Gyr. Once again it is possible to see the influence of the mass of the satellite on the intensity of the warp and the difference between the B and NB models. In B models, the interaction with the less massive satellites, in addition to preserving the bar, does not induce significant warp, while the merger with more massive satellites destroys the bar and causes S-shaped distortion. In these visualizations, the disk is aligned with the x-axis, but this may not be the best orientation for observing warp details in all cases. The same can be said about the time chosen. One of the best examples of an S-shaped warp is the M3R1 model (also shown in Figure 17, at the beginning of this section) with the disk aligned with the x-axis and at $t = 13$ Gyr, which is why in these figures we have chosen this orientation and time for all the models. Another result that becomes clear is that the interactions of the central galaxies with the satellites did not induce U-shaped warps.

We also examined the possibility of finding a correlation between the orientation of the warp and the orientation of the bar. The orientation of the bar $\theta_{\rm bar}$ is given by the equation (12):

Figure 26 – A_1 for all perturbed models of the non-barred galaxy. Note the different ranges in the colorbars.

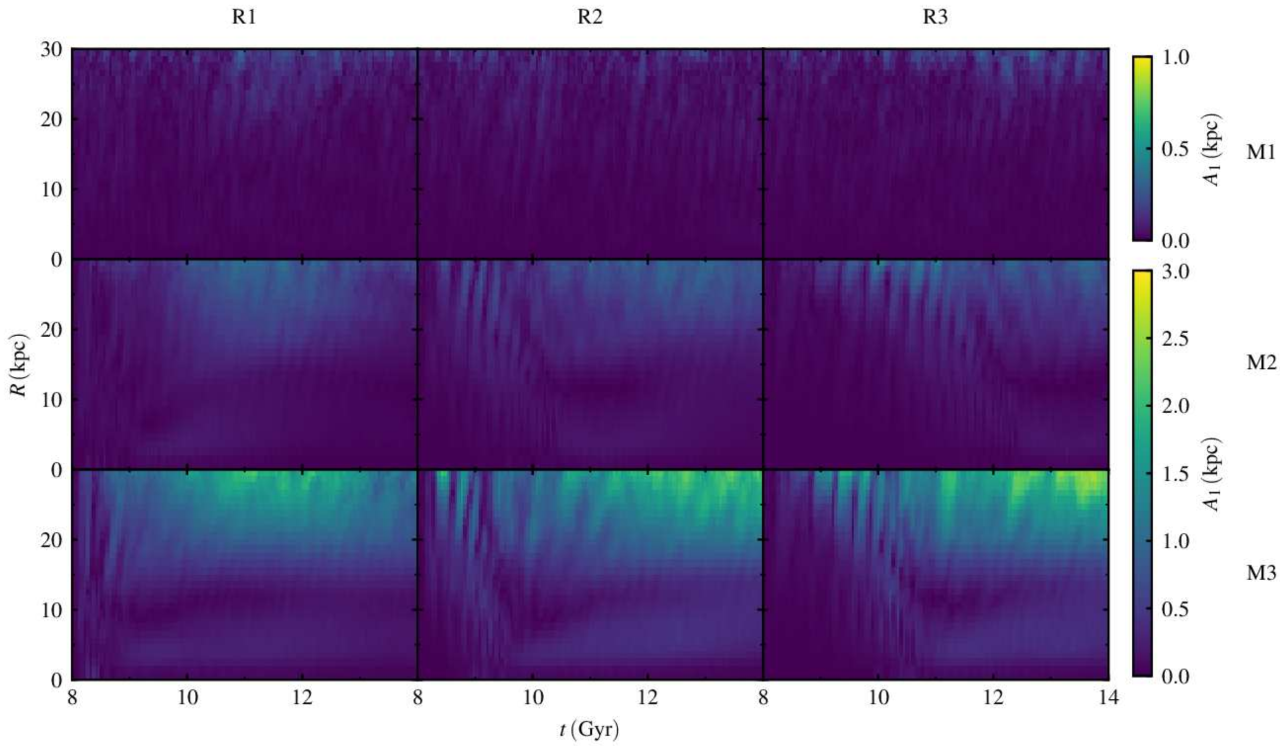

Source: The author (2024).

Figure 27 – A_1 for isolated B and NB models.

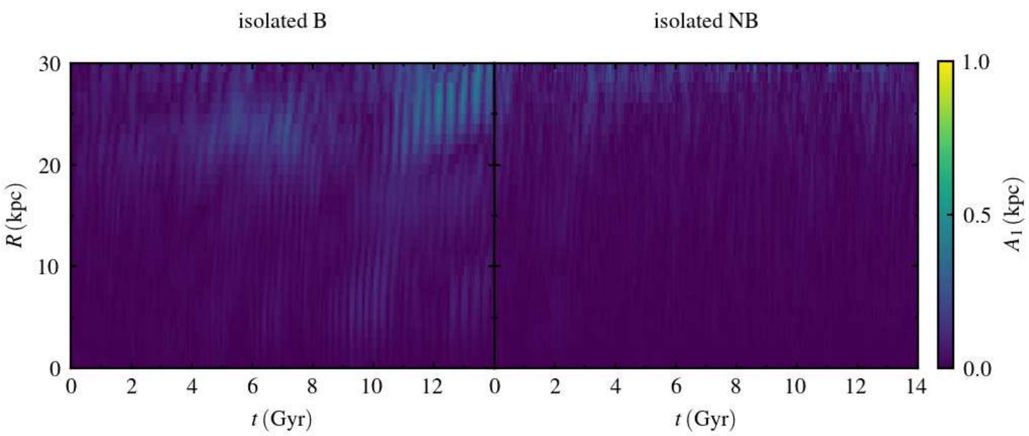

Source: The author (2024).

Figure 28 – Egde-on morphologies of the disks of barred galaxies after interaction with satellites at t = 13 Gyr.

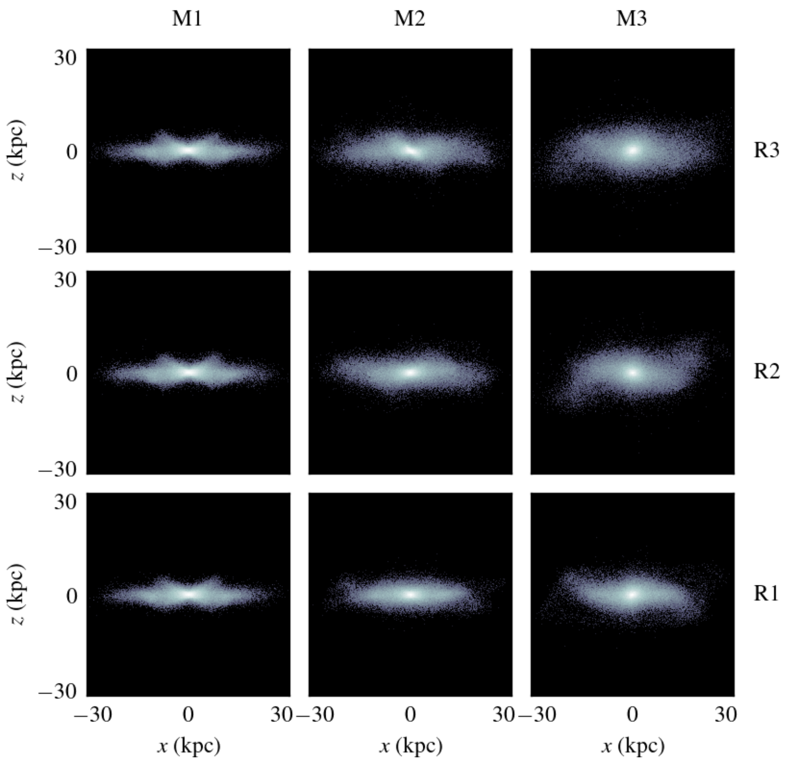

Source: The author (2024).

Figure 29 – Egde-on morphologies of the disks of non-barred galaxies after interaction with satellites at t = 13 Gyr.

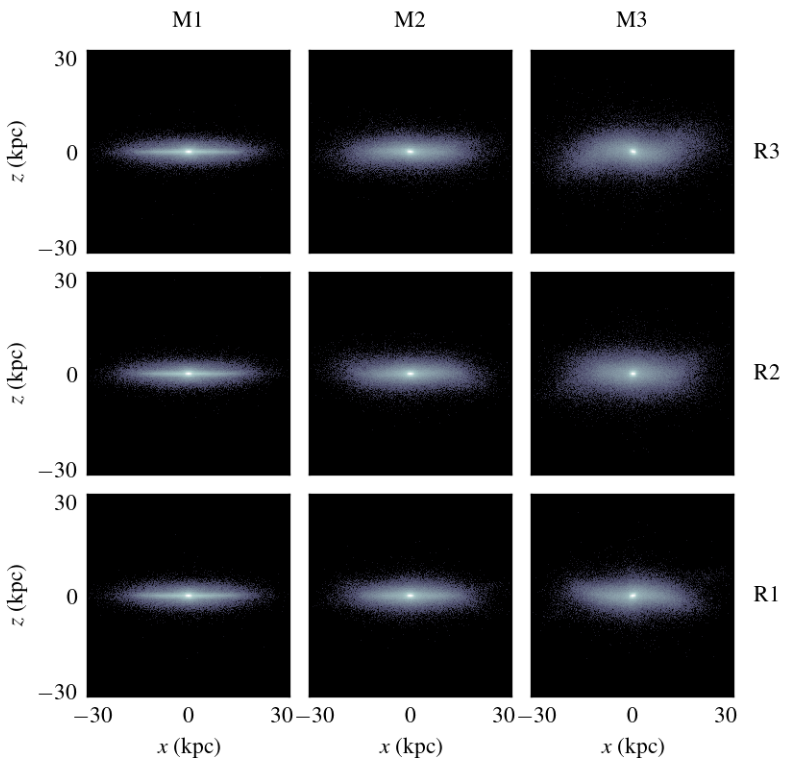

Source: The author (2024).

$$\tan\theta_{\text{bar}} = \frac{b_2}{a_2} \tag{12}$$

with a_2 and b_2 defined by equations (5) and (6). The warp orientation θ_{warp} is calculated in the same way, but with a_1 and b_1 determined by the equations (9) and (10). Our analysis found no correlation between θ_{bar} and θ_{warp}, i.e. the maximum intensity of the warp is neither preferentially aligned with the bar nor perpendicular to it. In the appendix A.5, we provide more details about this result.

3.3 GAS REPLACEMENT EXPERIMENT

All the measurements of warp intensity indicated in which of the central galaxy models the warp signal is stronger. As these models differ in just two aspects – the presence of gas and the presence of a bar, we needed to check if any changes in the warp were really due to the morphology of the galaxy or if the gas has some influence. Therefore we carried out a test, preparing a second version of the NB-M2R2 model, replacing all the gas particles with disk particles at the start of the simulation (t = 8 Gyr). This altered model has evolved up to 14 Gyr and we saved outputs every 0.05 Gyr, as we did with all the other simulations.

Figure 30 shows the mean height maps comparing the original and the altered NB-M2R2 models with the B-M2R2 model. At the end of the simulation, in t = 14 Gyr, there is almost no difference between the NB models. To understand the evolution of warp in these models over time, we also analyzed the evolution of maximum amplitude of warp W, showed in Figure 31. The warp intensity is slightly lower in the gas-free model compared to the original, during the most part of the simulation, but the W values are similar at the beginning and end. Most importantly, both NB models have a lower warp intensity in comparison with the barred galaxy. These results indicate that it is not the presence of gas that inhibits vertical asymmetries in NB models.

3.4 DISCUSSION

Certainly our models cannot represent the variety of properties that the bars in real galaxies exhibit. In this study, we focused on the contrast between a galaxy with a strong, long bar (model B) and a galaxy without a bar (model NB). Erwin (2005) found that bars in lenticular galaxies (SB0) and early-type spirals (SBa and SBb) galaxies are larger than those in late-type spirals (SBc and SBd). The author also analyzed some studies on simulations and

Figure 30 – Maps of mean heights at $t = 14$ Gyr comparing the models perturbed by a satellite of mass $0.5 \times 10^{10} M_{\odot}$ and orbital radius 20 kpc. From left to right there is the barred galaxy B-M2R2, the original non-barred galaxy NB-M2R2 and this same model but with the gas particles replaced by stars (NB-M2R2 (no gas)). B-M2R2 and NB-M2R2 models have already been shown in Figures 20 and 21.

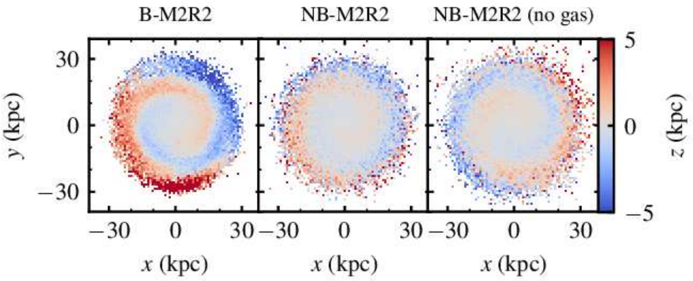

Source: The author (2024).

Figure 31 – Evolution of maximum amplitude of warp W for models perturbed by a satellite of mass $0.5 \times 10^{10} M_{\odot}$ and orbital radius 20 kpc. B-M2R2 and NB-M2R2 models have already been shown in Figure 23.

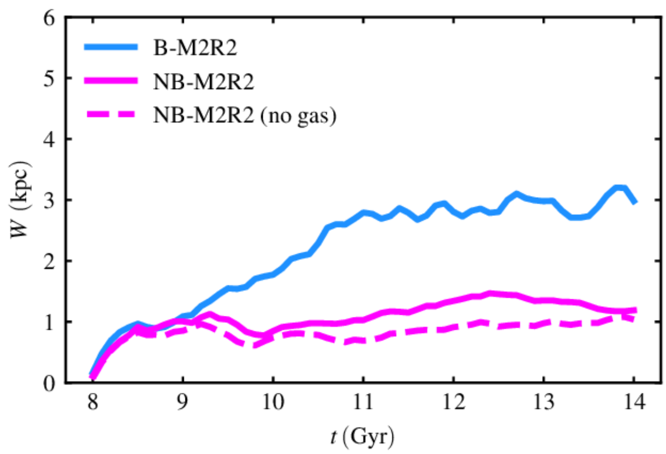

Source: The author (2024).

concluded that simulations often produce long bars, like those seen in SB0-SBb galaxies. This is consistent with studies (e.g. ATHANASSOULA; MISIRIOTIS, 2002) that indicate that bars appear spontaneously in N-body simulations. Erwin (2019) argued that the dependence of bar size on Hubble type can be explained as a side effect of stellar mass and Hubble type correlations. Longer bars are seen in larger, massive galaxies, and later Hubble types have a tendency to be smaller and lower in mass than early-type spirals. Based on this analysis, it seems reasonable to consider that our model B represents early-type barred spirals. It represents an extreme case. Other barred galaxies, of varying strengths and sizes, would be in an intermediate regime between models B and NB. The elliptical isophote fitting method for measuring bar size could be used in model B to compare typical bar length values in SB0-SBb galaxies, for example.

In our simulations, the bar in the B models has undergone changes during the interactions. We used the $m = 2$ mode of the projected mass distribution to calculate the bar strength A_2 and found that the mass and orbital radius of the satellite determined the fate of the bar of the central galaxy. The satellites of mass M1 did not change the development of the bar; the satellites of mass M2 made it weaker and smaller; and the satellites of mass M3 destroyed it. These impacts on the bar occurred earlier in the case of fly-bys of satellites with orbital radius R1, later in interactions with satellites of orbital radius R2, and even later in minor mergers with satellites of orbital radius R3.

These results are consistent with the findings of Ghosh *et al.* (2021), which conclude that bar weakening is common in minor merger events, and Athanassoula (2003a), which argues that the evolution of interacting galaxies depends strongly on the density of the satellite, leading to its destruction (if it has low mass) or to the bar destruction (if it is massive). Zana *et al.* (2018) show that bars can be resilient and recover their strength after a fly-by with a satellite, however, in our simulations, there are several passages of the satellite. At the end of the orbit, in most models (except in M1R3 and M1R2), the perturber is absorbed into the disk of the central galaxy. Therefore, there is no recovery in the bar strength.

We used spherical satellites, but other results could have emerged if their shape had been different. Ghosh *et al.* (2021) performed simulations with a barred central galaxy interacting with disk and spheroidal dwarf galaxies, and they conclude that spheroidal satellites are more impactful in weakening the bar because they are more efficient in the process of bringing stellar particles within the bar region.

Both B and NB models developed warps induced by satellites. We quantified the intensity of the asymmetries by comparing mean height maps, analyzing the peaks in the azimuthal height profile W and measuring the intensity of the bending mode A_1. W captures a specific intensity for each instant of time. We found that the measurement is not extremely sensitive to the choice of radial ring. On the other hand, A_1 has the advantage of providing radial information at each instant of time. However, it ideally captures a dipole-type bending mode, but in our models, the warp has a spiral appearance for most of its evolution, so its orientation and intensity is not well defined at all instants.

Despite these restrictions, our study demonstrated that the characteristics of the satellite have a systematic impact on the induced warps. Satellites of mass M1 cause very small asymmetries in the central galaxies and satellites of masses M2 and M3 induce notable warps, but the ones with the greatest amplitude are the result of interaction with satellites of mass M3. The radial information provided by A_1 shows that the satellites of orbital radius R1 induce distortions in the center and edges of the disk at same time, in the beginning of the simulation; meanwhile, satellites of orbital radius R2 and R3 first distort the edges, and later, the asymmetries also appear in the center.

In Gómez *et al.* (2017) magneto-hydrodynamics simulations, warps have several causes besides interaction with satellites, and the galaxies interacted with more than one satellite. Despite the differences compared to this study, a common result is the influence of massive satellites in inducing more intense warps: in Gómez *et al.* (2017), galaxies with strong vertical patterns interacted at least once with a satellite with mass $\sim 10^{10.5} M_{\odot}$ during the last $\sim$ 5 Gyr. Grand *et al.* (2016) also concluded that massive satellites (masses $> 10^{10} M_{\odot}$) were relevant for vertical disk heating in their simulations of Milky Way-like galaxies. The inclination of the orbit of the satellite is also a factor that can impact the intensity of the induced warp. Semczuk *et al.* (2020) found that the angle between the orbital angular momentum of the satellite and the angular momentum of the central galaxy that most preferentially lead to warp formation is $\sim 45°$. In our analysis, all orbits are polar, so we were not able to compare how the intensity of the warp varies in relation to this aspect.

The main result of our analysis is that the induced warps are always stronger in the B models in comparison with the NB ones. This fact applies to all perturbed models and even to the isolated models: in agreement with Chequers and Widrow (2017), our isolated barred galaxy shows a subtle warp signal (at $t \sim 10$ Gyr), without any interaction. The difference between the B and NB models must not be due to the gas, since we did a test with one of the perturbed NB models replacing gas particles with stars and still the non-barred galaxy continued to suffer less warp. So it was not the presence of gas that was inhibiting intense warp. Another conclusion in common with Chequers and Widrow (2017) is that bending waves should be long-lived features in disk galaxies. In our simulations, the induced warps last for several Gyr.

The warp of the Milky Way may be the result of interaction with the Sagittarius dwarf spheroidal galaxy (Sgr) (LAPORTE *et al.*, 2018; BLAND-HAWTHORN; TEPPER-GARCÍA, 2021; POGGIO *et al.*, 2021). It might be interesting to find parallels between the warps induced by the satellites in this study and the observational data from the Galactic warp. However, even for studies that aim to model Sgr orbital history, it is hard to deal with uncertainties on its parameters, as the progenitor mass (Sgr lost mass as it crossed the disk of the Milky Way) and the distance in pericentric passages. The simulations in Laporte *et al.* (2018), for example, established models of Sgr with masses of $6 \times 10^{10}\mathrm{M}_\odot$ and $1 \times 10^{11}\mathrm{M}_\odot$ crossing the Milky Way disk several times in the last 7 Gyr. During the interaction, the satellite causes the material in the disk to be excited to heights of $|z| \sim 5$ kpc to 10 kpc. Although the warp amplitudes in our simulations are in this range, many parameters are different. In addition, in Laporte *et al.* (2018) the Large Magellanic Cloud is also pointed out as an influence on the induced vertical asymmetries. In conclusion, the warp of the Milky Way and all its interactions are too complex to be compared directly with our study.

4 CONCLUSIONS

In this study, we use N-body simulations to investigate the susceptibility of barred and non-barred galaxies to develop warps induced by satellites. Our models were composed of a central spiral galaxy (B and NB models) and spherical satellites with varying masses (M1, M2 and M3) and orbital radii (R1, R2 and R3). We analyzed how the interactions between the galaxies impact the development of the bar and the formation of warps. Our main findings are listed below:

- In the interactions between satellites and the barred central galaxy, the bar can be preserved, weakened or destroyed. The level of bar weakening is determined by the mass of the satellite. And the time it takes depends on the initial orbital radius of the satellite.
- Warps in barred and non-barred galaxies are induced by the interaction with satellites. The mass of the perturber is the main influence on the intensity of the warp. These vertical asymmetries appear strongly at the edges and more weakly in the central regions. The initial orbital radius of the satellite determines when they will appear in the innermost part of the central galaxy.
- Warps are always stronger in the barred galaxies in comparison with the non-barred galaxies, in perturbed and isolated models.

In future studies, it would be interesting to explore models with satellite orbits of different inclinations and check their impact on the bar weakening and warp formation. The parameter space with galaxies with bars of different intensities, representing other Hubble types, could also be investigated. In addition, the elliptical isophote fitting method can be used to measure the length of the bar in different models. Additional analysis of the vertical frequencies of the orbits may clarify the mechanism responsible for the response of a barred galaxy to external disturbances.

REFERÊNCIAS

AGUERRI, J. A. L.; MÉNDEZ-ABREU, J.; CORSINI, E. M. The population of barred galaxies in the local universe. I. Detection and characterisation of bars. **A&A**, v. 495, n. 2, p. 491–504, fev. 2009.

AGUERRI, J. A. L. *et al.* Characterizing bar structures: application to NGC 1300, NGC 7479 and NGC 7723. **A&A**, v. 361, p. 841–849, set. 2000.

ALONSO, S.; COLDWELL, G.; LAMBAS, D. G. AGN spiral galaxies in groups: effects of bars. **A&A**, v. 572, p. A86, dez. 2014.

ANN, H. B.; PARK, J. C. Warped disks in spiral galaxies. **NA**, v. 11, n. 4, p. 293–305, jan. 2006.

APPEL, A. W. An Efficient Program for Many-Body Simulation. **SIAM Journal on Scientific and Statistical Computing**, v. 6, n. 1, p. 85–103, jan. 1985.

ATHANASSOULA, E. Bar-Halo Interaction and Bar Growth. **ApJL**, v. 569, n. 2, p. L83–L86, abr. 2002.

ATHANASSOULA, E. Isolated and Interacting Galaxies: Simulations with GRAPE. *In*: Makino, J.; Hut, P. (Ed.). **Astrophysical Supercomputing using Particle Simulations**. *[S.l.: s.n.]*, 2003. v. 208, p. 177.

ATHANASSOULA, E. What determines the strength and the slowdown rate of bars? **MNRAS**, v. 341, n. 4, p. 1179–1198, jun. 2003.

ATHANASSOULA, E. *et al.* Orbits as building blocks of a barred galaxy model. **A&A**, v. 127, n. 2, p. 349–360, nov. 1983.

ATHANASSOULA, E.; MACHADO, R. E. G.; RODIONOV, S. A. Bar formation and evolution in disc galaxies with gas and a triaxial halo: morphology, bar strength and halo properties. **MNRAS**, v. 429, n. 3, p. 1949–1969, mar. 2013.

ATHANASSOULA, E.; MISIRIOTIS, A. Morphology, photometry and kinematics of N -body bars - I. Three models with different halo central concentrations. **MNRAS**, v. 330, n. 1, p. 35–52, fev. 2002.

BARAZZA, F. D.; JOGEE, S.; MARINOVA, I. Bars in Disk-dominated and Bulge-dominated Galaxies at z ~0: New Insights from ~3600 SDSS Galaxies. **ApJ**, v. 675, n. 2, p. 1194–1212, mar. 2008.

BARNES, J.; HUT, P. A hierarchical O(N log N) force-calculation algorithm. **Nature**, v. 324, n. 6096, p. 446–449, dez. 1986.

BINNEY, J. Warps. **ARAA**, v. 30, p. 51–74, jan. 1992.

BLAND-HAWTHORN, J.; TEPPER-GARCÍA, T. Galactic seismology: the evolving 'phase spiral' after the Sagittarius dwarf impact. **MNRAS**, v. 504, n. 3, p. 3168–3186, jul. 2021.

BOURNAUD, F.; COMBES, F.; SEMELIN, B. The lifetime of galactic bars: central mass concentrations and gravity torques. **MNRAS**, v. 364, n. 1, p. L18–L22, 11 2005.

BRUNTHALER, A. *et al.* The Bar and Spiral Structure Legacy (BeSSeL) survey: Mapping the Milky Way with VLBI astrometry. **Astronomische Nachrichten**, v. 332, n. 5, p. 461, jun. 2011.

BURKE, B. F. Systematic distortion of the outer regions of the galaxy. **AJ**, v. 62, p. 90, maio 1957.

CHENG, X. *et al.* Exploring the Galactic Warp through Asymmetries in the Kinematics of the Galactic Disk. **ApJ**, v. 905, n. 1, p. 49, dez. 2020.

CHEQUERS, M. H.; WIDROW, L. M. Spontaneous generation of bending waves in isolated Milky Way-like discs. **MNRAS**, v. 472, n. 3, p. 2751–2763, dez. 2017.

CHROBÁKOVÁ, Ž.; NAGY, R.; LÓPEZ-CORREDOIRA, M. Structure of the outer Galactic disc with Gaia DR2. **A&A**, v. 637, p. A96, maio 2020.

COMBES, F.; SANDERS, R. H. Formation and properties of persisting stellar bars. **A&A**, v. 96, p. 164–173, mar. 1981.

CONSELICE, C. J. The Evolution of Galaxy Structure Over Cosmic Time. **ARAA**, v. 52, p. 291–337, ago. 2014.

CONTE, Z. A. L. *et al.* A JWST investigation into the bar fraction at redshifts $1 \leq z \leq 3$. **MNRAS**, v. 530, n. 2, p. 1984–2000, maio 2024.

COSTANTIN, L. *et al.* A Milky Way-like barred spiral galaxy at a redshift of 3. **Nature**, v. 623, n. 7987, p. 499–501, nov. 2023.

CUI, Y. *et al.* A spatial-color layout feature for representing galaxy images. *In*: **IEEE Winter Conference on Applications of Computer Vision**. *[S.l.: s.n.]*, 2014. p. 213–219.

CUOMO, V. *et al.* Bar pattern speeds in CALIFA galaxies. II. The case of weakly barred galaxies. **A&A**, v. 632, p. A51, dez. 2019.

DAS, M. *et al.* Central Mass Concentration and Bar Dissolution in Nearby Spiral Galaxies. **ApJ**, v. 582, n. 1, p. 190–195, jan. 2003.

DEBATTISTA, V. P. *et al.* The Secular Evolution of Disk Structural Parameters. **ApJ**, v. 645, n. 1, p. 209–227, jul. 2006.

DEBATTISTA, V. P.; SELLWOOD, J. A. Dynamical Friction and the Distribution of Dark Matter in Barred Galaxies. **ApJL**, v. 493, n. 1, p. L5–L8, jan. 1998.

DEBATTISTA, V. P.; SELLWOOD, J. A. Constraints from Dynamical Friction on the Dark Matter Content of Barred Galaxies. **ApJ**, v. 543, n. 2, p. 704–721, nov. 2000.

DEHNEN, W.; SEMCZUK, M.; SCHÖNRICH, R. A twisted and precessing Cepheid warp in the outer Milky Way disc. **MNRAS**, v. 523, n. 1, p. 1556–1564, jul. 2023.

ELMEGREEN, B. G.; ELMEGREEN, D. M. Properties of barred spiral galaxies. **ApJ**, v. 288, p. 438–455, jan. 1985.

ERWIN, P. How large are the bars in barred galaxies? **MNRAS**, v. 364, n. 1, p. 283–302, nov. 2005.

ERWIN, P. The dependence of bar frequency on galaxy mass, colour, and gas content - and angular resolution - in the local universe. **MNRAS**, v. 474, n. 4, p. 5372–5392, mar. 2018.

ERWIN, P. What determines the sizes of bars in spiral galaxies? **MNRAS**, v. 489, n. 3, p. 3553–3564, 08 2019.

ESKRIDGE, P. B. *et al.* The Frequency of Barred Spiral Galaxies in the Near-Infrared. **AJ**, v. 119, n. 2, p. 536–544, fev. 2000.

EVENT HORIZON TELESCOPE COLLABORATION *et al.* First Sagittarius A* Event Horizon Telescope Results. I. The Shadow of the Supermassive Black Hole in the Center of the Milky Way. **ApJL**, v. 930, n. 2, p. L12, maio 2022.

GAIA COLLABORATION *et al.* The Gaia mission. **A&A**, v. 595, p. A1, nov. 2016.

GARCÍA-CONDE, B. *et al.* Galactoseismology in cosmological simulations. Vertical perturbations by dark matter, satellite galaxies, and gas. **A&A**, v. 683, p. A47, mar. 2024.

GARCÍA-RUIZ, I.; SANCISI, R.; KUIJKEN, K. Neutral hydrogen and optical observations of edge-on galaxies: Hunting for warps. **A&A**, v. 394, p. 769–789, nov. 2002.

GENEL, S. *et al.* Introducing the Illustris project: the evolution of galaxy populations across cosmic time. **MNRAS**, v. 445, n. 1, p. 175–200, 09 2014.

GHOSH, S. *et al.* Fate of stellar bars in minor merger of galaxies. **MNRAS**, v. 502, n. 2, p. 3085–3100, abr. 2021.

GILMORE, G.; REID, N. New light on faint stars - III. Galactic structure towards the South Pole and the Galactic thick disc. **MNRAS**, v. 202, p. 1025–1047, mar. 1983.

GINGOLD, R. A.; MONAGHAN, J. J. Smoothed particle hydrodynamics: theory and application to non-spherical stars. **MNRAS**, v. 181, p. 375–389, nov. 1977.

GÓMEZ, F. A. *et al.* Warps and waves in the stellar discs of the Auriga cosmological simulations. **MNRAS**, v. 465, n. 3, p. 3446–3460, mar. 2017.

GRAND, R. J. J. *et al.* Vertical disc heating in Milky Way-sized galaxies in a cosmological context. **MNRAS**, v. 459, n. 1, p. 199–219, jun. 2016.

GUO, Y. *et al.* First Look at z > 1 Bars in the Rest-frame Near-infrared with JWST Early CEERS Imaging. **ApJL**, v. 945, n. 1, p. L10, mar. 2023.

HAN, J. J. *et al.* Tilted Dark Halos Are Common and Long-lived, and Can Warp Galactic Disks. **ApJL**, v. 957, n. 2, p. L24, nov. 2023.

HART, R. E. *et al.* Galaxy Zoo: comparing the demographics of spiral arm number and a new method for correcting redshift bias. **MNRAS**, v. 461, n. 4, p. 3663–3682, out. 2016.

HERNQUIST, L. An Analytical Model for Spherical Galaxies and Bulges. **ApJ**, v. 356, p. 359, jun. 1990.

HOHL, F. Numerical Experiments with a Disk of Stars. **ApJ**, v. 168, p. 343, set. 1971.

HOU, L. G.; HAN, J. L. The observed spiral structure of the Milky Way. **A&A**, v. 569, p. A125, set. 2014.

HOZUMI, S. Destructible Bars in Disk Galaxies under the Dynamical Influence of a Massive Central Black Hole. **PASJ**, v. 64, p. 5, fev. 2012.

HUANG, Y. *et al.* On the Kinematic Signature of the Galactic Warp As Revealed By the LAMOST-TGAS Data. **ApJ**, v. 864, n. 2, p. 129, set. 2018.

HUBBLE, E. P. A spiral nebula as a stellar system, Messier 31. **ApJ**, v. 69, p. 103–158, mar. 1929.

HUBBLE, E. P. **Realm of the Nebulae**. *[S.l.]*: Yale University Press, 1936.

IDETA, M.; HOZUMI, S. Bar Dissolution in Prolate Halos. **ApJL**, v. 535, n. 2, p. L91–L94, jun. 2000.

IVEZIĆ, Ž. *et al.* LSST: From Science Drivers to Reference Design and Anticipated Data Products. **ApJ**, v. 873, n. 2, p. 111, mar. 2019.

KERR, F. J. A Magellanic effect on the galaxy. **AJ**, v. 62, p. 93–93, maio 1957.

KHACHATURYANTS, T. *et al.* Bending waves excited by irregular gas inflow along warps. **MNRAS**, v. 512, n. 3, p. 3500–3519, maio 2022.

LAPORTE, C. F. P. *et al.* The influence of Sagittarius and the Large Magellanic Cloud on the stellar disc of the Milky Way Galaxy. **MNRAS**, v. 481, n. 1, p. 286–306, nov. 2018.

LEAVITT, H. S. 1777 variables in the Magellanic Clouds. **Annals of Harvard College Observatory**, v. 60, p. 87–108, jan. 1908.

LEE, Y. H.; ANN, H. B.; PARK, M.-G. Bar Fraction in Early- and Late-type Spirals. **ApJ**, v. 872, n. 1, p. 97, fev. 2019.

LIN, C. C.; SHU, F. H. On the Spiral Structure of Disk Galaxies. **ApJ**, v. 140, p. 646, ago. 1964.

ŁOKAS, E. L. Formation of Tidally Induced Bars in Galactic Flybys: Prograde versus Retrograde Encounters. **ApJ**, v. 857, n. 1, p. 6, abr. 2018.

ŁOKAS, E. L. Anatomy of a buckling galactic bar. **A&A**, v. 629, p. A52, set. 2019.

ŁOKAS, E. L. Buckling instability in tidally induced galactic bars. **A&A**, v. 624, p. A37, abr. 2019.

LUCY, L. B. A numerical approach to the testing of the fission hypothesis. **AJ**, v. 82, p. 1013–1024, dez. 1977.

MACHADO, R. E. G.; ATHANASSOULA, E. Loss of halo triaxiality due to bar formation. **MNRAS**, v. 406, n. 4, p. 2386–2404, ago. 2010.

MARINOVA, I.; JOGEE, S. Characterizing Bars at z ~0 in the Optical and NIR: Implications for the Evolution of Barred Disks with Redshift. **ApJ**, v. 659, n. 2, p. 1176–1197, abr. 2007.

MARTINEZ-VALPUESTA, I.; SHLOSMAN, I. Why Buckling Stellar Bars Weaken in Disk Galaxies. **ApJ**, v. 613, n. 1, p. L29, aug 2004.

MARTINEZ-VALPUESTA, I.; SHLOSMAN, I.; HELLER, C. Evolution of Stellar Bars in Live Axisymmetric Halos: Recurrent Buckling and Secular Growth. **ApJ**, v. 637, n. 1, p. 214–226, jan. 2006.

MARZIANI, P. Grand challenges in Milky Way and galaxies. **Frontiers in Astronomy and Space Sciences**, v. 2, p. 1–4, 2015.

MÉNDEZ-ABREU, J. *et al.* The Nature and Nurture of Bars and Disks. **ApJL**, v. 761, n. 1, p. L6, dez. 2012.

MENÉNDEZ-DELMESTRE, K. *et al.* A Near-Infrared Study of 2MASS Bars in Local Galaxies: An Anchor for High-Redshift Studies. **ApJ**, v. 657, n. 2, p. 790–804, mar. 2007.

NAIR, P. B.; ABRAHAM, R. G. A Catalog of Detailed Visual Morphological Classifications for 14,034 Galaxies in the Sloan Digital Sky Survey. **ApJ**, v. 186, n. 2, p. 427–456, fev. 2010.

NAIR, P. B.; ABRAHAM, R. G. On the fraction of barred spiral galaxies. **ApJL**, v. 714, n. 2, p. L260, apr 2010.

OSTRIKER, J. P.; PEEBLES, P. J. E. A Numerical Study of the Stability of Flattened Galaxies: or, can Cold Galaxies Survive? **ApJ**, v. 186, p. 467–480, dez. 1973.

PATSIS, P. A.; KAUFMANN, D. E. Resonances and the morphology of spirals in N-body simulations. **A&A**, v. 352, p. 469–478, dez. 1999.

PESCHKEN, N.; ŁOKAS, E. L. Tidally induced bars in Illustris galaxies. **MNRAS**, v. 483, n. 2, p. 2721–2735, 12 2018.

PFENNIGER, D. The 3D dynamics of barred galaxies. **A&A**, v. 134, n. 2, p. 373–386, maio 1984.

POGGIO, E. *et al.* Evidence of a dynamically evolving Galactic warp. **Nature Astronomy**, v. 4, p. 590–596, mar. 2020.

POGGIO, E. *et al.* The kinematic signature of the Galactic warp in Gaia DR1. I. The Hipparcos subsample. **A&A**, v. 601, p. A115, maio 2017.

POGGIO, E. *et al.* Measuring the vertical response of the Galactic disc to an infalling satellite. **MNRAS**, v. 508, n. 1, p. 541–559, nov. 2021.

PRIETO, M. *et al.* Optical surface photometry of a sample of disk galaxies. II. Structural components. **A&A**, v. 367, p. 405–427, fev. 2001.

RAHA, N. *et al.* A dynamical instability of bars in disk galaxies. **Nature**, v. 352, n. 6334, p. 411–412, ago. 1991.

RESHETNIKOV, V.; COMBES, F. Statistics of optical WARPS in spiral disks. **A&A**, v. 337, p. 9–16, set. 1998.

ROBERTS, W. W. Large-Scale Shock Formation in Spiral Galaxies and its Implications on Star Formation. **ApJ**, v. 158, p. 123, out. 1969.

ROBERTSON, B. E. Galaxy Formation and Reionization: Key Unknowns and Expected Breakthroughs by the James Webb Space Telescope. **ARAA**, v. 60, p. 121–158, ago. 2022.

ROGSTAD, D. H.; SHOSTAK, G. S. Gross Properties of Five Scd Galaxies as Determined from 21-CENTIMETER Observations. **ApJ**, v. 176, p. 315, set. 1972.

ROMERO-GÓMEZ, M. *et al.* Gaia kinematics reveal a complex lopsided and twisted Galactic disc warp. **ApJ**, v. 627, p. A150, jul. 2019.

ROSAS-GUEVARA, Y. *et al.* The rise and fall of bars in disc galaxies from z = 1 to z = 0. The role of environment. **A&A**, v. 684, p. A179, abr. 2024.

RUBIN, V. C.; FORD, W. K. Rotation of the Andromeda Nebula from a Spectroscopic Survey of Emission Regions. **ApJ**, v. 159, p. 379, fev. 1970.

RUGGIERO, R.; NETO, G. B. L. The fate of the gaseous discs of galaxies that fall into clusters. **MNRAS**, v. 468, n. 4, p. 4107–4115, 03 2017.

SAKAMOTO, K. *et al.* Bar-driven Transport of Molecular Gas to Galactic Centers and Its Consequences. **ApJ**, v. 525, n. 2, p. 691–701, nov. 1999.

SÁNCHEZ-MARTÍN, P.; ROMERO-GÓMEZ, M.; MASDEMONT, J. J. Warp evidence in precessing galactic bar models. **A&A**, v. 588, p. A76, abr. 2016.

SÁNCHEZ-SAAVEDRA, M. L.; BATTANER, E.; FLORIDO, E. Frequency of warped spiral galaxies at visible wavelengths. **MNRAS**, v. 246, p. 458, out. 1990.

SCHAYE, J. *et al.* The EAGLE project: simulating the evolution and assembly of galaxies and their environments. **MNRAS**, v. 446, n. 1, p. 521–554, jan. 2015.

SCHÖNRICH, R.; DEHNEN, W. Warp, waves, and wrinkles in the Milky Way. **MNRAS**, v. 478, n. 3, p. 3809–3824, ago. 2018.

SELLWOOD, J. A. Bar Instability in Disk-Halo Systems. **ApJ**, v. 819, n. 2, p. 92, mar. 2016.

SEMCZUK, M. *et al.* Tidally induced warps of spiral galaxies in IllustrisTNG. **MNRAS**, v. 498, n. 3, p. 3535–3548, nov. 2020.

SHAPLEY, H.; CURTIS, H. D. The Scale of the Universe. **Bulletin of the National Research Council**, v. 2, n. 11, p. 171–217, maio 1921.

SHEN, J.; SELLWOOD, J. A. The Destruction of Bars by Central Mass Concentrations. **ApJ**, v. 604, n. 2, p. 614–631, abr. 2004.

SHEN, J.; ZHENG, X.-W. The bar and spiral arms in the Milky Way: structure and kinematics. **RAA**, v. 20, n. 10, p. 159, out. 2020.

SHETH, K. *et al.* Evolution of the Bar Fraction in COSMOS: Quantifying the Assembly of the Hubble Sequence. **ApJ**, v. 675, n. 2, p. 1141–1155, mar. 2008.

SHETH, K. *et al.* Secular Evolution via Bar-driven Gas Inflow: Results from BIMA SONG. **ApJ**, v. 632, n. 1, p. 217–226, out. 2005.

SHIELDS, G. A. A Brief History of Active Galactic Nuclei. **PASP**, v. 111, n. 760, p. 661–678, jun. 1999.

SILVA-LIMA, L. A. *et al.* Revisiting the role of bars in AGN fuelling with propensity score sample matching. **A&A**, v. 661, p. A105, maio 2022.

SMITH, R. W. Beyond the Galaxy: The Development of Extragalactic Astronomy 1885-1965: Part 1. **Journal for the History of Astronomy**, v. 39, n. 134, p. 91–119, fev. 2008.

SMITH, R. W. Beyond the Galaxy: The Development of Extragalactic Astronomy 1885-1965: Part 2. **Journal for the History of Astronomy**, v. 40, p. 71–107, jan. 2009.

SODI, B. C. Stellar, Gas, and Dark Matter Content of Barred Galaxies. **ApJ**, v. 835, n. 1, p. 80, jan. 2017.

SPARKE, L. S.; GALLAGHER, J. S. **Galaxies in the Universe: An Introduction**. *[S.l.]*: Cambrigde University Press, 2007.

SPRINGEL, V. E pur si muove: Galilean-invariant cosmological hydrodynamical simulations on a moving mesh. **MNRAS**, v. 401, n. 2, p. 791–851, jan. 2010.

SPRINGEL, V. *et al.* Simulating cosmic structure formation with the gadget-4 code. **MNRAS**, v. 506, n. 2, p. 2871–2949, 07 2021.

SPRINGEL, V. *et al.* Simulations of the formation, evolution and clustering of galaxies and quasars. **Nature**, v. 435, n. 7042, p. 629–636, jun. 2005.

SWART, J. G. de; BERTONE, G.; DONGEN, J. van. How dark matter came to matter. **Nature Astronomy**, v. 1, p. 0059, mar. 2017.

TEPPER-GARCÍA, T.; BLAND-HAWTHORN, J.; FREEMAN, K. Galactic seismology: joint evolution of impact-triggered stellar and gaseous disc corrugations. **MNRAS**, v. 515, n. 4, p. 5951–5968, out. 2022.

TEPPER-GARCÍA, T.; BLAND-HAWTHORN, J.; LI, D. The M31/M33 tidal interaction: a hydrodynamic simulation of the extended gas distribution. **MNRAS**, v. 493, n. 4, p. 5636–5647, abr. 2020.

TOOMRE, A. On the gravitational stability of a disk of stars. **ApJ**, v. 139, p. 1217–1238, maio 1964.

TOOMRE, A.; TOOMRE, J. Galactic Bridges and Tails. **ApJ**, v. 178, p. 623–666, dez. 1972.

VALENZUELA, O.; KLYPIN, A. Secular bar formation in galaxies with a significant amount of dark matter. **MNRAS**, v. 345, n. 2, p. 406–422, out. 2003.

VARELA-LAVIN, S. *et al.* Lopsided galaxies in a cosmological context: a new galaxy-halo connection. **MNRAS**, v. 523, n. 4, p. 5853–5868, ago. 2023.

VAUCOULEURS, G. de. Revised Classification of 1500 Bright Galaxies. **ApJS**, v. 8, p. 31, abr. 1963.

VILLA-VARGAS, J.; SHLOSMAN, I.; HELLER, C. Dark Matter Halos and Evolution of Bars in Disk Galaxies: Varying Gas Fraction and Gas Spatial Resolution. **ApJ**, v. 719, n. 2, p. 1470–1480, ago. 2010.

WEGG, C.; GERHARD, O.; PORTAIL, M. The structure of the Milky Way's bar outside the bulge. **MNRAS**, v. 450, n. 4, p. 4050–4069, jul. 2015.

WEINBERG, M. D. Evolution of barred galaxies by dynamical friction. **MNRAS**, v. 213, n. 3, p. 451–471, 04 1985.

WOZNIAK, H. *et al.* Disc galaxies with multiple triaxial structures. I. BVRI and Hα surface photometry. **A&AS**, v. 111, p. 115, maio 1995.

YOACHIM, P.; DALCANTON, J. J. Structural Parameters of Thin and Thick Disks in Edge-on Disk Galaxies. **AJ**, v. 131, n. 1, p. 226–249, jan. 2006.

ZANA, T. *et al.* Bar resilience to flybys in a cosmological framework. **MNRAS**, v. 479, n. 4, p. 5214–5219, out. 2018.

ZEE, W.-B. G. *et al.* Warped Disk Galaxies. I. Linking U-type Warps in Groups/Clusters to Jellyfish Galaxies. **ApJ**, v. 935, n. 1, p. 48, ago. 2022.

APÊNDICES

APÊNDICE A – ANÁLISES ADICIONAIS

A.1 EVOLUTION OF A_2 IN NB MODELS

In the section 3.1, the evolution of A_2 for the B models was shown (Figure 14). The same analysis was made for the NB models. Regardless of the perturber's mass or initial orbital radius, final A_2 remains low, because the isolated model of this galaxy never developed a bar. However, it is possible to see peaks of high A_2 values at the beginning of the interaction with the satellites. This is not the case of tidally induced bars (e.g. ŁOKAS, 2018; PESCHKEN; ŁOKAS, 2018). The passage of a satellite — especially the more massive and closer ones, as is clear in the Figure 32 — only causes non-axisymmetric redistribution and accumulation of mass in the central parts of the disk of the galaxy, but it is never bar-shaped. Figure 33 reveals the disk configuration of the NB-M3R1 model at a time corresponding to the first peaks (t = 8.2 Gyr).

Figure 32 – Evolution of bar strength in isolated and perturbed models of the non-barred galaxy.

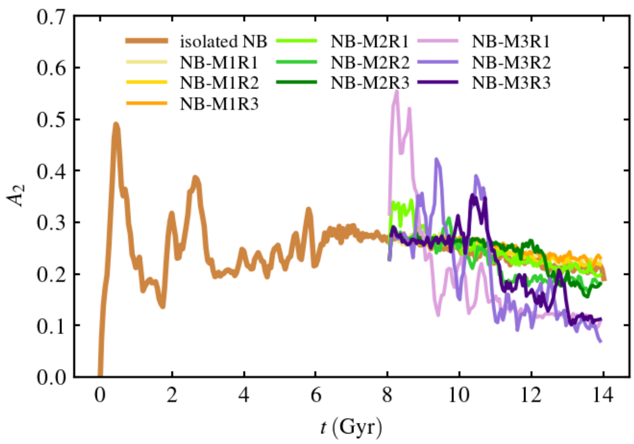

Source: The author (2024).

A.2 ORBITAL RADIUS AND A_2 EVOLUTION FOR M2 AND M3 MODELS

In the section 3.1, an example of orbital radius and A_2 evolution was shown only for model B-M2R2 (Figure 16). We showed that there are a temporal correlation between the greater proximity of the satellite and lower A_2 values. Here, in Figure 34, we present this result for all the other simulations with intermediate (M2) and massive (M3) satellites. This result does not apply to satellites with mass M1, since they do not cause a decrease in the bar strength because they are less massive, as already shown in Figure 14. Note the different axes for each variable

Figure 33 – Disk configuration after the interaction with a massive satellite (model NB-M3R1) at $t = 8.2$ Gyr.

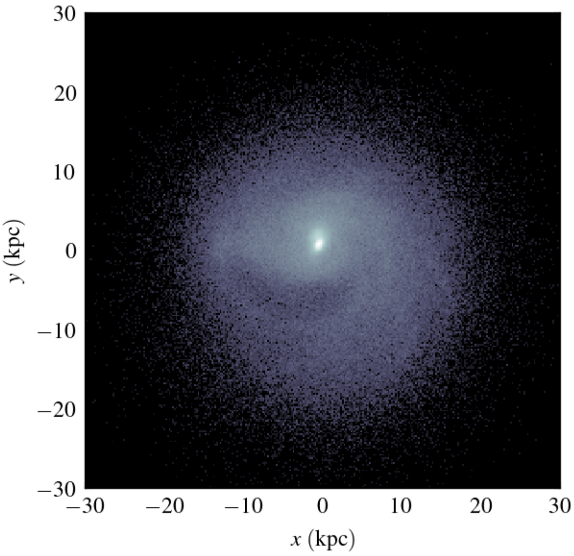

Source: The author (2024).

and also the different ranges on the axes, since each satellite has its initial orbital radius. It is also possible to see that the satellites are absorbed by the disk of the galaxy and are retained in its central region ($r \sim 5$ kpc).

Figure 34 – Orbital radius and A_2 evolution for M2 and M3 models.

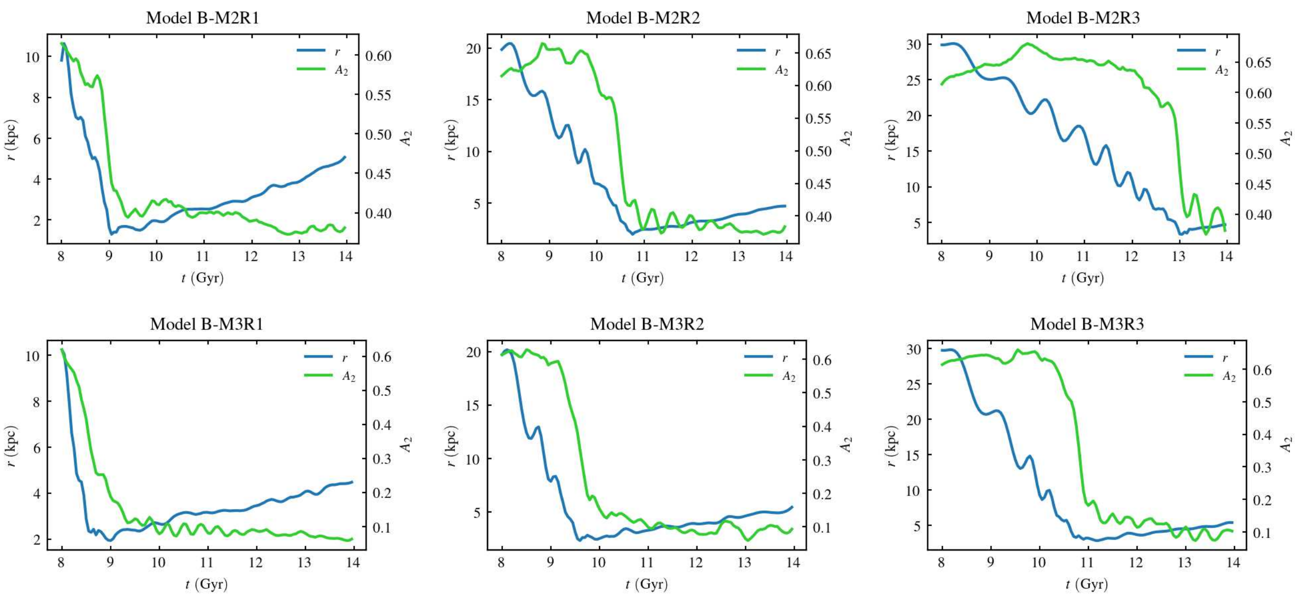

Source: The author (2024).

A.3 MEAN HEIGHTS MAPS FOR ALL MODELS

In the section 3.2, an example of a mean heights map was shown for one model (B-M3R1) (Figure 18). Here, the maps for all models, barred and non-barred, are presented in Figures 35, 36 and 37.

Figure 35 – Mean heights map for barred (left) and non-barred (right) galaxies perturbed by satellites with mass M1.

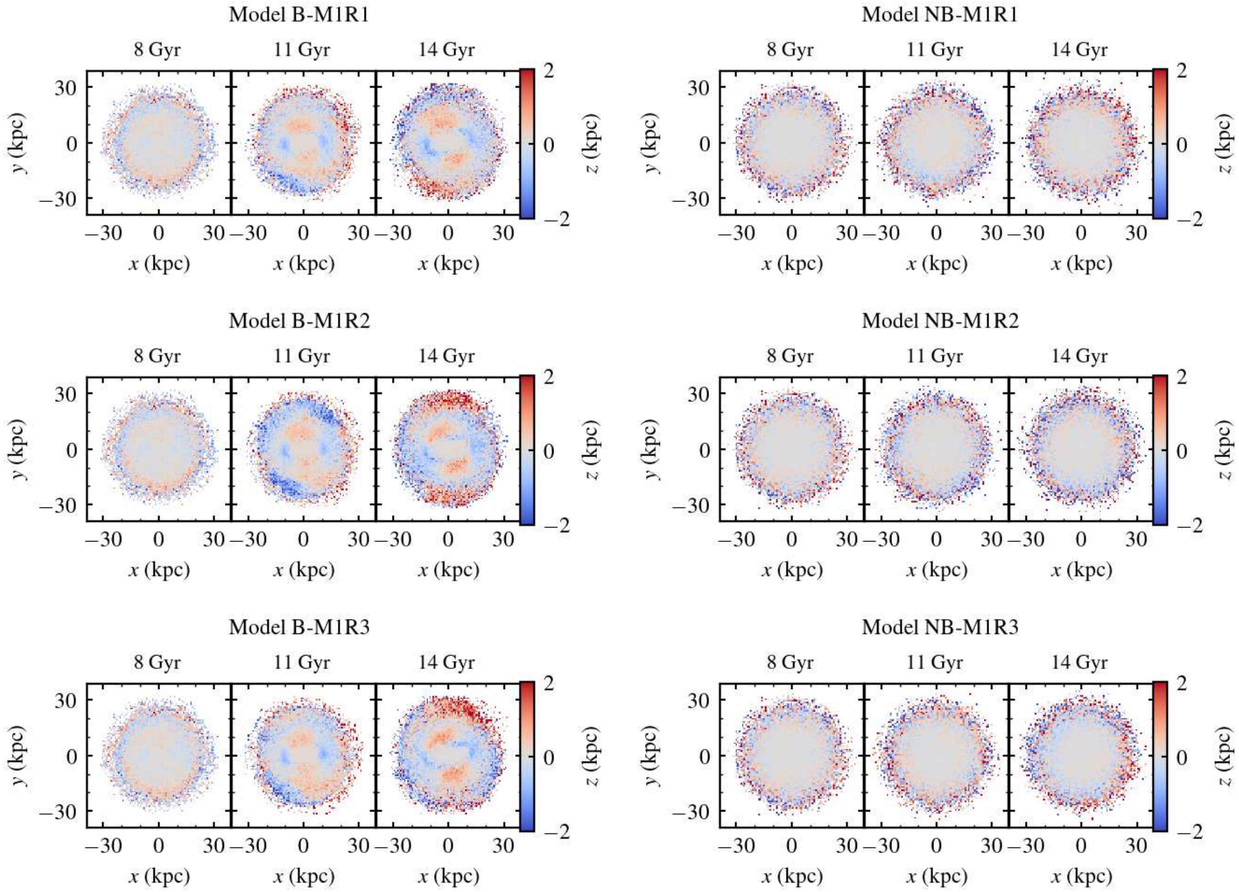

Source: The author (2024).

A.4 EVOLUTION OF W IN A MORE INTERNAL RING

In the section 3.2, Figure 23 showed the maximum amplitude of the warp W. The analysis was carried out in an outer ring of the disk ($20 < R < 30$ kpc). We tested the same measure for a more internal ring ($10 < R < 20$ kpc) and the pattern is the same: the warp is more intense in the B models in all cases, as presented in Figure 38.

Figure 36 – Mean heights map for barred (left) and non-barred (right) galaxies perturbed by satellites with mass M2.

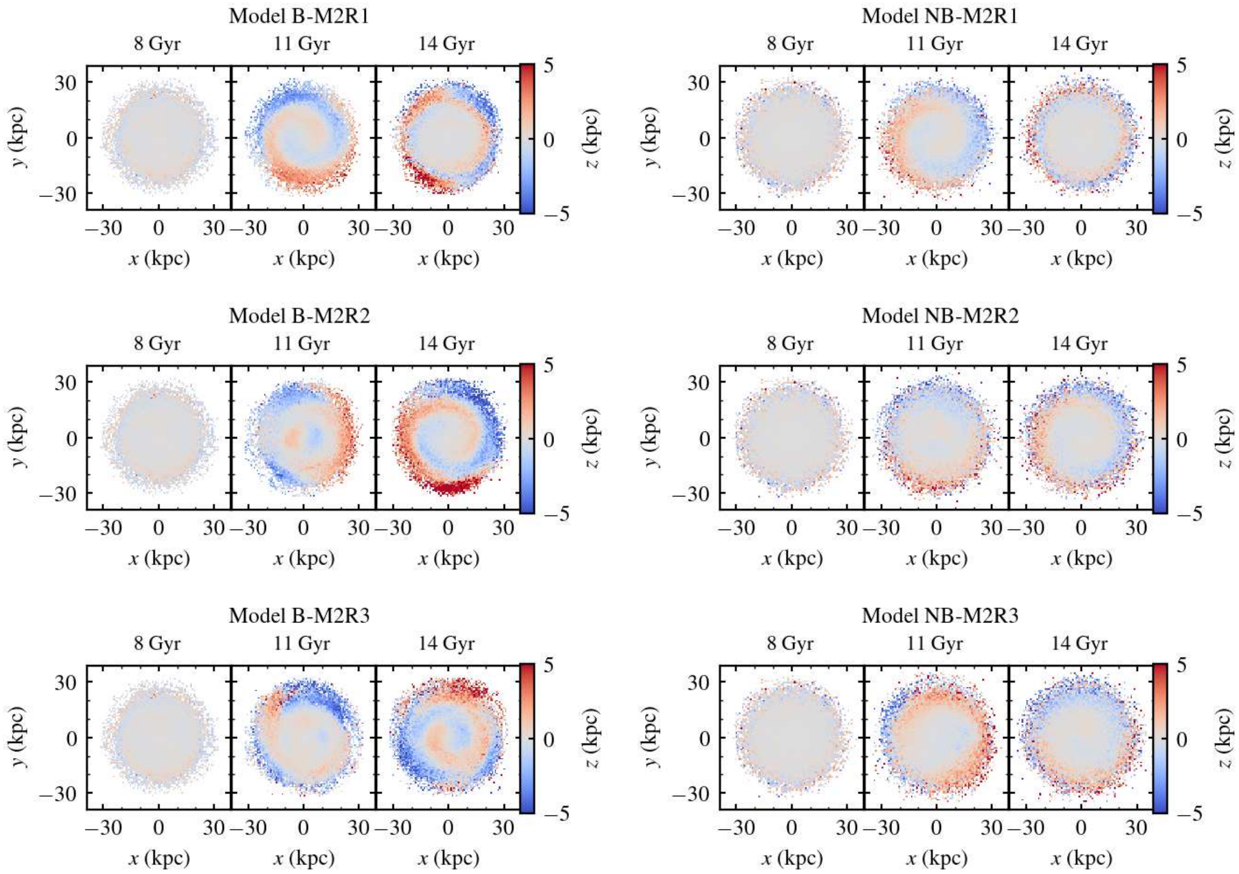

Source: The author (2024).

A.5 ORIENTATION OF THE WARP AND ORIENTATION OF THE BAR

In the section 3.2, it was suggested that there could be a correlation between the orientation of the bar (θ_{bar}) and the orientation of the warp (θ_{warp}). In our analysis, we found that θ_{warp} is clearly defined when the asymmetry is a strong dipole, which occurs in cases where the galaxy is perturbed by more massive satellites and/or at the end of the simulations, as shown in Figure 39 (left). The black line correctly indicates the orientation of the warp in model B-M3R1, at $t = 11$ Gyr. However, exactly in these cases, the bar is destroyed, so θ_{bar} may not be a reliable value (red line). On the other hand, the bar exists when the galaxy is perturbed by less massive satellites and/or when the simulation is still at the beginning. But then the warp is not yet well established or does not have a dipole shape, as the model M2R3 at $t = 9$ Gyr shown in Figure 39 (right).

Figure 37 – Mean heights map for barred (left) and non-barred (right) galaxies perturbed by satellites with mass M3.

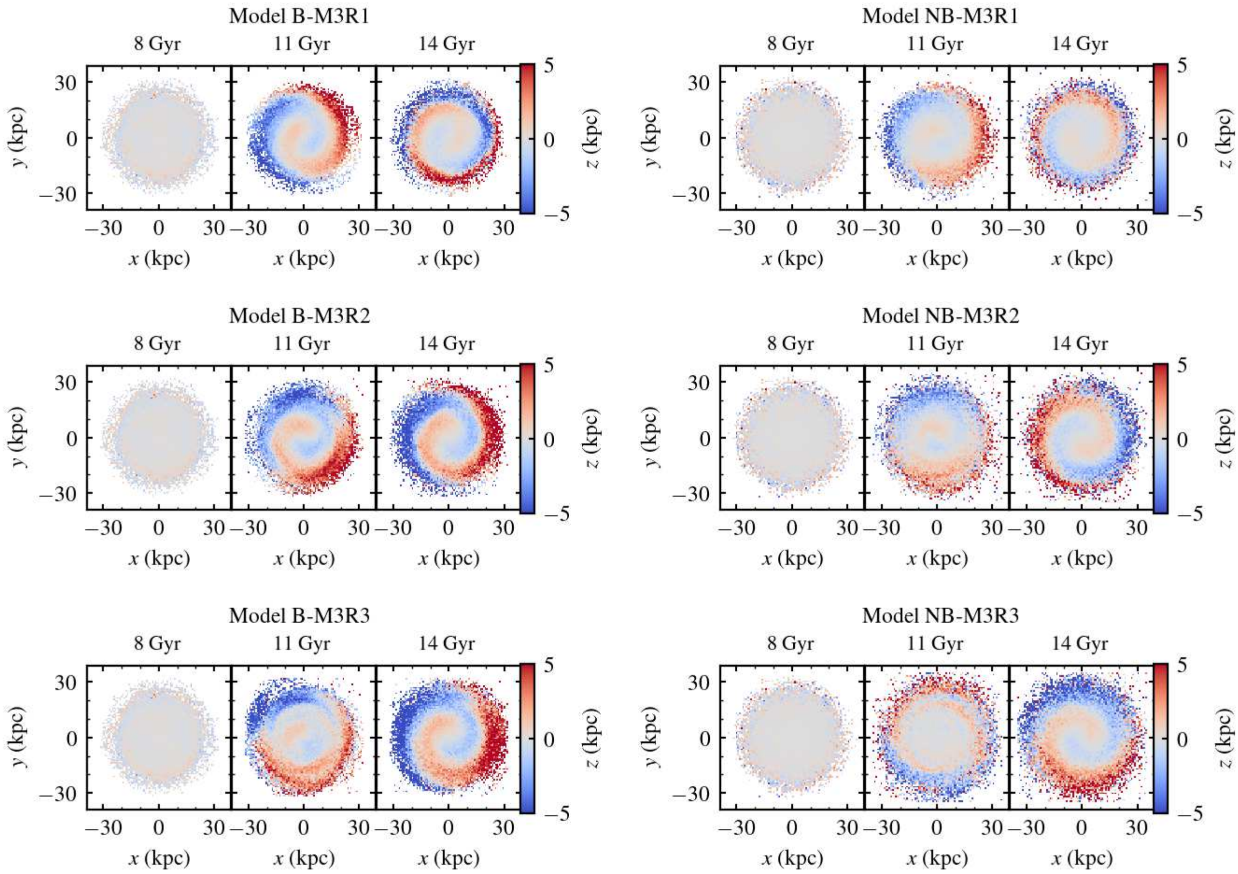

Source: The author (2024).

Figure 38 – Evolution of maximum amplitude of warp W for all perturbed models ($10 < R < 20$ kpc).

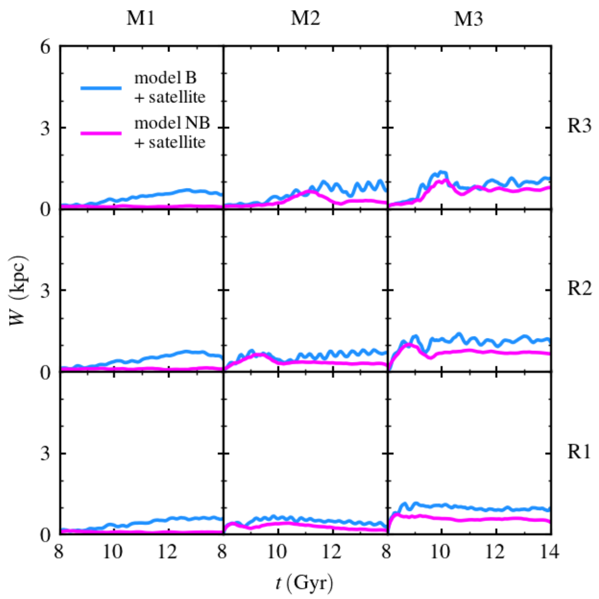

Source: The author (2024).

Figure 39 – Mean heights map for model B-M3R1 at t = 11 Gyr (left) and model B-M2R3 at t = 9 Gyr (right) with indication of warp and bar orientation.

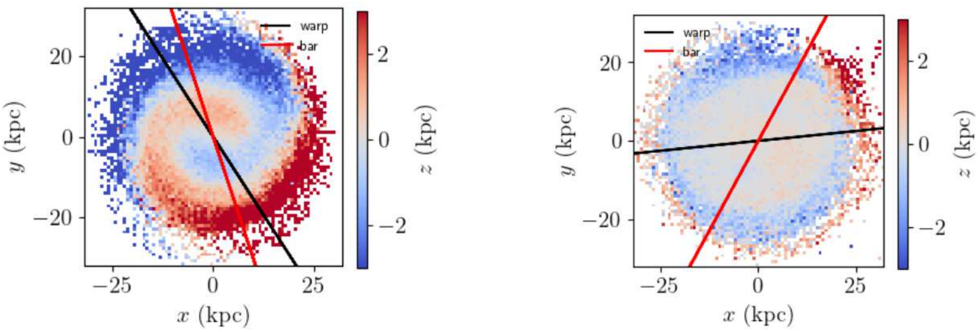

Source: The author (2024).

ANEXO

ANEXO A – OUTRAS PRODUÇÕES

Outras produções:

- Machado, R.E.G.; Sakamoto, K.R.; **Wille, A.**; Gonçalves, G.F. The Rotation of Classical Bulges in Barred Galaxies in the Presence of Gas. Universe 2024, 10, 223. https://doi.org/10.3390/universe10050223
- **Wille, A.**; Machado, R.E.G. Warped disks in simulated barred galaxies. XLVI Reunião da Sociedade Astronômica Brasileira. Boletim da Sociedade Astronômica Brasileira, 35, n. 1, p. 14-15, 2024.

Boletim da Sociedade Astronômica Brasileira, **35**, no. 1, 14-15

Warped disks in simulated barred galaxies

A. Wille[1] & R. E. G. Machado[1]

[1] Universidade Tecnológica Federal do Paraná, Curitiba, Brazil
e-mail: `andressawille@alunos.utpfr.edu.br`

Abstract. The close passage of dwarf galaxies can induce vertical asymmetries in the disk of the host galaxy. We aim to analyze the effects of warps induced by satellites on barred and non-barred galaxies, their evolution and amplitudes. In this study, we use *N*-body simulations of galaxies interacting with satellites of varying masses (0.1×10^{10}M$_\odot$, 0.5×10^{10}M$_\odot$ and 1×10^{10}M$_\odot$) and initial orbital distances (10, 20 and 30 kpc). We found that the vertical asymmetry will always be stronger in the barred galaxy, regardless of the mass or orbit of the perturber.

Resumo. A passagem próxima de galáxias anãs pode induzir assimetrias verticais no disco de galáxias. Nosso objetivo foi analisar os efeitos de warps induzidas por satélites em galáxias barradas e não barradas, sua evolução e amplitudes. Neste estudo, usamos simulações de *N*-corpos de galáxias interagindo com satélites de diferentes massas (0.1×10^{10}M$_\odot$, 0.5×10^{10}M$_\odot$ e 1×10^{10}M$_\odot$) e distâncias orbitais iniciais (10, 20 e 30 kpc). Constatamos que a assimetria vertical sempre será mais forte na galáxia barrada, independente da massa do perturbador.

Keywords. Galaxies: interactions – Galaxies: kinematics and dynamics – Galaxies: structure

1. Introduction

Bars are elongated structures in the center of spiral galaxies. Another feature that can appear on galactic disks are S-shaped warps, vertical asymmetries in which the disk has one side bent upwards and the other downwards. Possible explanations for this morphology include close passages the interaction with a satellite galaxy (e.g. Semczuk et al (2020)), that can also perturb the bar. In this study, we investigate the influence of the mass and the orbital radius of a satellite on the bar strength and on vertical asymmetries of the host galaxy: compared to a non-barred galaxy, is a barred galaxy more resilent against warping, or more succeptible to it?

2. Methods

We used the galstep code (Ruggiero & Lima Neto (2017)) to create the initial conditions and the Gadget-4 code (Springel et al (2021)) to run the simulations.

We first aimed to establish two models of galaxies: one strongly barred and one without bar. Since bars appear spontaneously in a large number of studies with N-body simulations (Athanassoula & Misiriotis (2002)), we tried varying different parameters in order to obtain a non-barred galaxy. We found that adding a high fraction of gas (75%) to the disk suppressed bar formation.

With the two models well established, we also ran simulations with the addition, at $t = 8$ Gyr, of satellites of different masses (0.1×10^{10}M$_\odot$, 0.5×10^{10}M$_\odot$ and 1×10^{10}M$_\odot$) and initial orbital radii (10, 20 and 30 kpc). The orbit chosen was a polar orbit in all cases.

In order to measure the bar strength (A_2), we used the coefficients of the Fourier series, quite sensitive to non-axisymmetric configurations. A_2 is given by equation 1:

$$A_2 = \max\left(\frac{\sqrt{a_2^2 + b_2^2}}{a_0}\right), \quad (1)$$

where a_n and b_n are shown by equations 2 and 3:

$$a_n(R) = \sum_{i=0}^{N_R} m_i \cos(n\,\theta),\ n = 0, 1, 2... \quad (2)$$

$$b_n(R) = \sum_{i=0}^{N_R} m_i \,\mathrm{sen}(n\,\theta),\ n = 1, 2... \quad (3)$$

with m_i being the mass in each ring i of radius R.

Fig. 1 shows A_2 and for barred and non-barred galaxies and the final disk configuration in each case.

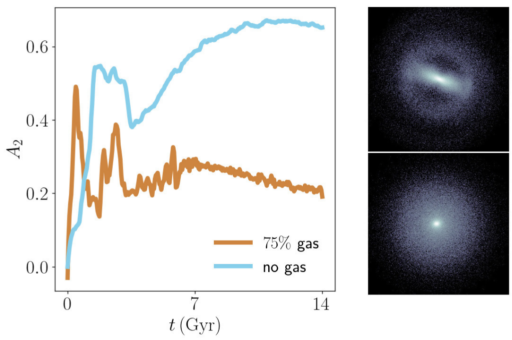

Figure 1. Left: evolution of bar strength. Right: appearance of the galaxies at 14 Gyr.

For the analysis of vertical asymmetries, we examined maps of the mean height z. Also, considering z in the outermost ring of the galactic disk (20 kpc $< r <$ 30 kpc), we calculated the mean of the highest point (peak) and the lowest point (valley) to find the maximum amplitude of the warp (A_{max}).

universe

MDPI

Article

The Rotation of Classical Bulges in Barred Galaxies in the Presence of Gas

Rubens E. G. Machado *, Kenzo R. Sakamoto, Andressa Wille and Gustavo F. Gonçalves

Departamento Acadêmico de Física, Universidade Tecnológica Federal do Paraná, Av. Sete de Setembro 3165, Curitiba 80230-901, PR, Brazil
* Correspondence: rubensmachado@utfpr.edu.br

Abstract: Barred galaxies often develop a box/peanut pseudobulge, but they can also host a nearly spherical classical bulge, which is known to gain rotation due to the bar. We aim to explore how the presence of gas impacts the rotation of classical bulges. We carried out a comprehensive set of hydrodynamical *N*-body simulations with different combinations of bulge masses and gas fractions. In these models, both massive bulges and high gas content tend to inhibit the formation of strong bars. For low-mass bulges, the resulting bar is stronger in cases of low gas content. In the stronger bar models, bulges acquire more angular momentum and thus display considerable rotational velocity. Such bulges also develop anisotropic velocity dispersions and become triaxial in shape. We found that the rotation of the bulge becomes less pronounced as the gas fraction is increased from 0 to 30%. These results indicate that the gas content has a significant effect on the dynamics of the classical bulge, because it influences bar strength. Particularly in the case of the low-mass bulges (10% bulge mass fraction), all of the measured rotational and structural properties of the classical bulge depend strongly and systematically on the gas content of the galaxy.

Keywords: galactic dynamics; barred galaxies; numerical simulations

check for updates

Citation: Machado, R.E.G.; Sakamoto, K.R.; Wille, A.; Gonçalves, G.F. The Rotation of Classical Bulges in Barred Galaxies in the Presence of Gas. *Universe* **2024**, *10*, 223. https://doi.org/10.3390/universe10050223

Academic Editor: Mauro D'Onofrio

Received: 3 April 2024
Revised: 7 May 2024
Accepted: 13 May 2024
Published: 16 May 2024

1. Introduction

In the central region of disk galaxies, a protuberance in the light distribution has been historically called a bulge. Bulges have long been understood to be similar to elliptical galaxies, since they are generally smooth spheroidal stellar structures dominated by random motion. To a first approximation, bulges even share with elliptical galaxies roughly the same $R^{1/4}$ radial profile of surface brightness. However, recent developments in the field indicate that bulges are more complicated and more diverse (see [1] for a review) than this early picture would have suggested. Moreover, bulges in general may hold important information to understand the formation and evolution of galaxies, both regarding early phases of hierarchical mergers and also more recent but long-term dynamical processes during secular evolution.

In particular, new classes of bulges have been identified and tentatively classified due to their peculiar structural and kinematic properties, and also stellar populations. Some bulges exhibit velocity structures that are more reminiscent of disks than ellipticals [2] e.g., in the sense that they are dominated more by rotation than by random motions. These classes of objects are sometimes called 'pseudobulges' in order to distinguish them from the 'classical bulges'.

Apart from disk-like bulges, a particularly interesting type of pseudobulges are the structures sometimes referred to as box/peanut (BP) bulges or box/peanut/X-shaped (BPX) bulges. Such X-shapes can be detected in observations of edge-on galaxies [3,4] e.g., They are now understood to be the product of bar formation and evolution. Specifically, simulations [5] reveal that a BPX morphology emerges when a strongly barred galaxy is viewed side-on, i.e., when the galactic disk is seen edge-on but additionally the longer axis